

RESEARCH

Open Access



# A1, an innovative fluorinated CXCR4 inhibitor, redefines the therapeutic landscape in colorectal cancer

Hossein Khorramdelazad<sup>1,2</sup>, Kowsar Bagherzadeh<sup>3</sup>, Ali Rahimi<sup>2,4</sup>, Ali Darehkordi<sup>5</sup>, Alireza Najafi<sup>2,4</sup>, Milad Karimi<sup>2,4</sup>, Majid Khoshmirsafa<sup>2,4</sup>, Gholamhossein Hassanshahi<sup>6</sup>, Elaheh Safari<sup>2,4\*</sup> and Reza Falak<sup>2,4\*</sup>

## Abstract

**Background** Colorectal cancer (CRC) is a globally prevalent malignancy, primarily affecting the colon and rectum, characterized by uncontrolled cellular changes in the intestinal wall lining. Recent evidence underlines the significant role of the CXCL12/CXCR4 axis in the development of CRC, suggesting that inhibiting this pathway could be a promising therapeutic approach. This study focuses on investigating the potential of N, N"-thiocarbonylbis (N'-(3,4-dimethyl phenyl)-2,2,2-trifluoroacetimidamide) (A1), a novel fluorinated CXCR4 inhibitor, through a comprehensive analysis encompassing *in silico*, *in vitro*, and *in vivo* studies.

**Methods** The molecular dynamic simulation method was employed to compute A1 binding affinity and energy for the CXCR4 receptor compared to AMD3100. *In vitro* experiments utilized the CT-26 mouse CRC cell line to compare the inhibitory effects of A1 and AMD3100 on tumor cell proliferation and migration. Following the development of the CRC animal model in BALB/c mice, immune system responses within the tumor microenvironment (TME) were evaluated. Flow cytometry and real-time PCR (RT-PCR) were used to measure the effects of AMD3100 and A1 on regulatory T-cell (Treg) infiltration and the expression of *CXCR4*, vascular endothelial growth factor (*VEGF*), fibroblast growth factors (*FGF*), interleukin-10 (*IL-10*), and tumor growth factor-beta (*TGF-β*) genes in tumor tissue. Additionally, enzyme-linked immunosorbent assay (ELISA) and immunohistochemistry (IHC) techniques were employed to assess VEGF, IL-10, and TGF-β tissue levels at the protein level.

**Results** Molecular dynamic simulation studies with molecular mechanics Poisson-Boltzman surface area (MM-PBSA) analysis revealed that A1 exhibits significantly lower binding energy for the CXCR4 receptor than AMD3100. A1 effectively inhibited the proliferation of CT-26 cells, significantly reduced tumor cell migration, attenuated Treg infiltration, and suppressed IL-10 and TGF-β expression at both mRNA and protein levels *in vivo*. Notably, A1 outperformed AMD3100 in reducing tumor size and increasing survival rate in treated animals, with minimal side effects.

**Conclusion** These findings emphasize the potential of A1 as a favorable anti-tumor small molecule in CRC. Further validation through rigorous preclinical and clinical studies may position A1 as a promising alternative to AMD3100 in human cancers.

**Keywords** AMD3100, Colorectal cancer, CXCR4 inhibitor, CXCL12, Fluorine

\*Correspondence:

Elaheh Safari

[el.safari@yahoo.com](mailto:el.safari@yahoo.com)

Reza Falak

[Falakr@iums.ac.ir](mailto:Falakr@iums.ac.ir); [rezafalak@gmail.com](mailto:rezafalak@gmail.com)

Full list of author information is available at the end of the article



© The Author(s) 2024. **Open Access** This article is licensed under a Creative Commons Attribution-NonCommercial-NoDerivatives 4.0 International License, which permits any non-commercial use, sharing, distribution and reproduction in any medium or format, as long as you give appropriate credit to the original author(s) and the source, provide a link to the Creative Commons licence, and indicate if you modified the licensed material. You do not have permission under this licence to share adapted material derived from this article or parts of it. The images or other third party material in this article are included in the article's Creative Commons licence, unless indicated otherwise in a credit line to the material. If material is not included in the article's Creative Commons licence and your intended use is not permitted by statutory regulation or exceeds the permitted use, you will need to obtain permission directly from the copyright holder. To view a copy of this licence, visit <http://creativecommons.org/licenses/by-nc-nd/4.0/>.

## Introduction

Colorectal cancer (CRC) stands as a prominent global health concern, affecting the colon and rectum with considerable morbidity and mortality [1]. The intricate interplay of various cellular processes within the intestinal wall gives rise to the uncontrolled growth of malignant cells in CRC [2]. CRC stands as the second leading cause of cancer-related deaths worldwide, mainly affecting men below the age of 50 [3]. More than half of the reported cases and fatalities are associated with modifiable risk factors like smoking, obesity, unhealthy diet, excessive alcohol intake, and lack of physical activity [4]. Implementing preventive procedures, including regular screening, surveillance, and targeted high-quality treatment, can substantially decrease CRC incidence and mortality rates [4].

Recent strides in cancer research revealed the pivotal role of immune system mediators, such as chemokines, particularly the CXCL12/CXCR4 axis, in the pathogenesis of CRC [5, 6]. Chemokines are signaling proteins that play a crucial role in immune responses and cell trafficking [7–11]. In the context of CRC, the CXCL12 chemokine and its receptor CXCR4 emerge as critical players [10, 12]. The interaction between CXCL12 and CXCR4 contributes to the progression of CRC by influencing tumor cell proliferation, migration, and immune responses within the tumor microenvironment (TME) [13]. Understanding this dynamic interplay offers a promising avenue for targeted therapeutic interventions [14]. Moving beyond conventional treatments, the focus has shifted towards exploring novel therapeutic agents, such as small molecules, to tackle human malignancies, such as CRC [15, 16]. It has been revealed that administering AMD3100, a Food and Drug Administration (FDA)-approved drug, could decrease metastatic lesions and boost antitumor immune responses in CRC [15]. A novel derivative of such molecule, N, N'-thiocarbonylbis(N'-(3,4-dimethylphenyl)-2,2,2-trifluoroacetimidamide) (A1), has recently captured attention as a potent CXCR4 inhibitor [17]. Based on our previous study, this fluorinated small molecule holds promise in modulating the CXCL12/CXCR4 axis, presenting a potential breakthrough in treating CRC [17].

Our investigation into the complex landscape of CRC and its immunopathogenesis emphasizes the examination of fluorinated small molecules, particularly A1. It is essential to elucidate the molecular complexities and harness the therapeutic potential of these agents. The primary objective of this study is to establish a foundation for innovative strategies in the continual battle against CRC.

## Materials and methods

### Computational studies

#### *Molecular dynamic simulations (MDs)*

The molecular dynamic simulation technique was used to evaluate the interactions of A1 with CXCR4 *in silico*. The stability of the interactions between the CXCR4 receptor binding pocket participant amino acids was further studied and identified through molecular docking studies [17]. The behaviors of the crystallographic ligand (ITD), A1, and AMD3100 in the binding pocket were fully monitored during 100 ns of MDs using GROMACS software v5.1.5 [18] employing GROMOS AMBER force field (amber99sb-ildn) [19]. The initial conformations of CXCR4 in complex with ITD, A1, and AMD3100 were obtained from the models reported in the previous study [17]. The CXCR4 and the target complex with the desired targets were solvated in a dodecahedral box of TIP3P water molecules with a minimum distance of 14 Å between the protein surface and the box walls, and periodic boundary conditions were assigned in all directions. The system net charge was neutralized by replacing water molecules with appropriate counter sodium and chloride ions. The van der Waals cutoff was considered 14 Å. The solvated systems were minimized through the steepest descent algorithm with 1000 kJ mol<sup>-1</sup> nm<sup>-1</sup> tolerance followed by a canonical ensemble (NVT) for 20 ps and an isothermal-isobaric ensemble (NPT) in a periodic boundary condition. The system's temperature and pressure were maintained using the Berendsen thermostat [20] and the Parinello-Rahman barostat algorithm [21] at constant temperature and pressure of 310 K and 1 bar, respectively. The long-range electrostatic interactions were calculated using the particle mesh Ewald (PME) algorithm [22]. The LINCS algorithm [23] was applied to restrain all the bonds with an integration step of 1 fs. The whole system was subjected to 100 ns of molecular dynamic simulations at constant pressure and temperature. Further analysis was done over the coordinate files extracted from the trajectories.

#### *Binding free energy calculations*

The binding affinities of the target compounds for CXCR4 were studied using binding free energy calculations using the g\_mmpbsa tool and the MM-PBSA strategy [24] with GROMACS trajectories individually. The energy contribution of the key residues that bind the desired compounds was also computed.

### Graphical representation

Discovery Studio 4.1 [25], VMD 1.9.2 [26], and PyMOL 2.3.4 software [27] were applied to all graphical representations and molecular images.

### A1 synthesis

The chemical processes and compound synthesis steps have been described in our previous study [17]. Briefly, the synthesis of (N-(3,4-dimethylphenyl)-2,2,2-trifluoroacetimidoyl chloride) (2a) involved combining  $\text{Ph}_3\text{P}$ ,  $\text{Et}_3\text{N}$ , and TFA in a flask, followed by the addition of 3,4-dimethyl alanine in  $\text{CCl}_4$ . After refluxing and stirring for five hours, the solvent was evaporated, and the residue was processed to yield trifluoroacetimidoyl chloride. Subsequently, for the synthesis of N, N''-thiocarbonylbis(N'-(3,4-dimethylphenyl)-2,2,2-trifluoroacetimidamide) A1, thiourea and sodium hydrogen carbonate were mixed in ether, and N-(3,4-dimethylphenyl)-2,2,2-trifluoroacetimidoyl chloride (2a) was added dropwise. After refluxing and stirring, the reaction was monitored using TLC, and the solvent was removed under reduced pressure. The resulting mixture was filtered, and the crude product was further purified by dissolving in n-hexane and filtering. The final compound was obtained after removing the solvent under reduced pressure [17, 28] (Supplementary data, Figure S1). Additionally, in our previous study, fluorine, hydrogen, and carbon nuclear magnetic resonance spectroscopy ( $^{19}\text{F}$ -NMR,  $^1\text{H}$ -NMR, and  $^{13}\text{C}$ -NMR) as well as Fourier transform infrared spectroscopy (FT-IR) were used to characterize A1 [17].

### Cell lines & cell culture

The mouse embryonic fibroblast (MEF) cell line, which served as our control cells, and the CT-26 mouse CRC cells were purchased from the Pasteur Institute of Iran in Tehran. Cell lines were cultured in DMEM/F-12 (Dulbecco's Modified Eagle Medium/Nutrient Mixture F-12) (Gibco 12,500,062) and 10% fetal bovine serum (FBS) (Gibco A4766801). The cells were incubated at 37 °C with 5%  $\text{CO}_2$ .

### Gene expression assay

RT-PCR and flow cytometry were employed to explore how the CXCR4 receptor is expressed in CT-26 cells and compared with non-cancerous MEF cells.

According to the manufacturer's instructions, total RNA was extracted from CT-26 and MEF cells using an RNA extraction kit (Sinaclon EX6101, Iran). Spectrophotometry and gel agarose electrophoresis were employed to assess the purity and integrity of the extracted RNA. The optical density (OD) ratio of the purified RNA was

checked at 260 and 280 nm to ensure that they fell within the optimal range of 1.8 to 2 (Supplementary data, Figure S2). A one-step cDNA synthesis kit (KPG-cDNA 50, Iran) was used for cDNA synthesis following manufacturer instructions. In a dedicated RNase/DNase-free microtube, a mixture of 5  $\mu\text{L}$  of template RNA (ranging from 5 ng to 5  $\mu\text{g}$ ), one  $\mu\text{L}$  of either Oligo dT or Random hexamer primers, 14  $\mu\text{L}$  of Master mix, and RNase-free water to a total volume of 20  $\mu\text{L}$  was prepared. The solution underwent a temperature program of 10 min at 25 °C, 60 min at 47 °C, and 5 min at 95 °C, facilitating the conversion of RNA into cDNA.

The RT-PCR technique was used to detect gene expression alterations. Primer design for specific RNA sequences was accomplished using PrimerExpress™ version 3.2 software and verified through the NCBI Primer-BLAST tool. Primer sequences are shown in Table 1. Before RT-PCR, cDNA samples were normalized to 50 ng/ $\mu\text{L}$ . The assessment of target gene expression, encompassing *CXCR4*, was quantified within cell cultures. The 2xqPCRBIO SyGreen Mix Lo-ROX PB20.11-05-s (PCR Biosystem, England) was employed for quantification. Actin- $\beta$  served as the designated reference gene, and all reactions were executed in duplicate. The Rotor-Gene Q 2plex System (Qiagen) was utilized following the recommended protocol, involving an initial cycle of 95 °C for 2 min, followed by 40 cycles comprising denaturation at 95 °C for 5 s and annealing/extension at 60 °C for 25 s for template amplification. Additionally, a melting curve step was

**Table 1** Primer sequences and other details of the primers used in this study

Gene	Tm (°C)	Sequence
<i>CXCR4 F</i>	62.43	ACCTCTACAGCAGCGTTCTCATC
<i>CXCR4 R</i>	57.3	TGTTGGTGGCGTGGACAATA
<i>VEGF-A F</i>	61.4	CCAGACCTCTCACCGGAAAG
<i>VEGF-A R</i>	59.82	CTGTCAACGGTGACGATGATG
<i>FGF-2 F</i>	57.87	TGGTATGTGGCACTGAAACGA
<i>FGF-2 R</i>	56.67	TCCAGGTCCCCTTTTGGAT
<i>IL-10 F</i>	58.24	GATGCCCCAGGCAGAGAA
<i>IL-10 R</i>	57.3	CACCCAGGGAATTCAAATGC
<i>TGF-<math>\beta</math> F</i>	58.83	GCAGTGGCTGAACCAAGGA
<i>TGF-<math>\beta</math> R</i>	58.83	AGCAGTGAGCGCTGAATCG
<i>Actin <math>\beta</math> F</i>	55.25	GATGTATGAAGGCTTTGGTC
<i>Actin <math>\beta</math> R</i>	53.2	TGTGCACTTTTATTGGTCTC
<i>MMP-9 F</i>	59.3	AGTGGGACCATCATAACATCATAT
<i>MMP-9 R</i>	58.83	TCTCGCGCAAGTCTTCAG
<i>NFKB F</i>	58.8	TGGCCGTGGAGTACGACAA
<i>NFKB R</i>	58.8	GCATCACCCCTCCAGAAGCA

Tm: melting temperature

integrated into the final phase, involving 10 s at 95 °C and 10 s intervals at 0.2 °C enhancements spanning the temperature range from 62 to 95 °C.

#### Flow cytometry

Following the cell culture procedures outlined in previous sections, 500,000 MEF and CT-26 cells were mixed in 100 µL of staining buffer. This mixture added 2.5 µL of the PE-conjugated anti-mouse CXCR4-specific antibody (R&D systems FAB21651P). The cells were then incubated in the dark at 4 °C for 30 min. Post-incubation, a BD Bioscience FACScaliber flow cytometer (BD, USA) was employed to detect and analyze the percentage of CXCR4<sup>+</sup> cells. Furthermore, the impact of the A1 compound on the percentage of CXCR4<sup>+</sup> CT-26 cells was examined using flow cytometry. CT-26 cells were treated with a 60 µg/mL dose of A1 and 100 ng/mL of CXCL12 and incubated at 37 °C for 72 h. Subsequently, 50,000 cells were mixed with 100 µL of staining buffer. Then, 2.5 µL of PE-conjugated specific CXCR4 antibodies were added to the microtubes. The cells were incubated for 30 min in the dark at 4 °C. Then, we evaluated the percentage of CXCR4<sup>+</sup> cells using a BD Bioscience FACScaliber flow cytometer (BD, USA).

#### Proliferation assay

An MTT assay kit (Sigma, 298-93-1, Germany) was employed to evaluate the impact of AMD3100 and A1 on cell proliferation. For CT-26 cells in a 96-well plate, a cell density of 5000 cells per well was established, with an optimal culture medium volume of 200 µL per well. Initially, CT-26 cells were plated with 100 µL of FBS-free DMEM medium per well in 96-well culture plates. Following overnight incubation, varying concentrations of AMD3100 (APExBIO, A2025, USA) and A1 were dissolved in 100 µL of medium and introduced to the respective wells. The optimal concentration of A1 and AMD3100 was determined to be 40 µg/mL based on examination of various concentrations. In addition, 100 ng/mL of CXCL12 as a proliferation stimulator and ligand of CXCR4 was added to each well. After 24, 48, and 72 h of treatment, 10 µL of sterile MTT solution (5 mg/mL) was added to each well and incubated for 3 h. Subsequently, the supernatant was removed, and 150 µL of dimethyl sulfoxide (DMSO) (Sigma, 67–68-5, Germany) was added to each well, followed by shaking for 20 min at 37 °C. The absorbance at 570 nm was measured using an ELISA microplate reader (BioTech, USA). Notably, A1 and AMD3100 were soluble in H<sub>2</sub>O with gentle warming.

#### Functional assays

Functional assays were employed to confirm the binding of the compound to the CXCR4 receptor and to investigate the changes in the downstream pathway of the CXCL12/CXCR4 axis. The expression of CXCR4, matrix metalloproteinase-9 (*MMP-9*), and nuclear factor kappa B (*NFκB*) genes was assessed in two treatment groups, one with a 60 µg/mL concentration of A1 and AMD3100 (based on our previous study and obtained IC<sub>50</sub> concentration) and the other with a control group, in the presence and absence of 100 ng/mL CXCL12 [17].

#### cAMP assay

Additionally, considering the role of the CXCL12/CXCR4 axis in reducing cAMP concentration, the cAMP assay was conducted using a competitive ELISA method in two treated groups with different concentrations of A1 and AMD3100 (10, 100, and 1000 nm/mL) using a cAMP ELISA kit (R&D Systems, KGE002B). Initially, CT-26 cells were seeded at a density of 10<sup>6</sup> × 5 cells per well and cultured for 24 h in DMEM/F-12 medium under FBS-deprived conditions. Subsequently, the cells in all groups were stimulated with 5 µM of forskolin (Sigma, F3917) for 30 min. Following the stimulation, each sample was treated with A1 and AMD3100 at concentrations of 10, 100, and 1000 nm/mL for 30 min [29]. After this stage, the cells were incubated for an additional 30 min with 150 ng/mL of recombinant CXCL12 protein (R&D systems, BLB041604), and they were then prepared for the ELISA step according to the manufacturer's instructions.

#### Western blotting

Western blotting was used to measure the protein expression of pAKT as one of the most critical adaptor molecules in the CXCL12/CXCR4 signaling pathway and confirm CXCR4 inhibition by A1 compared with AMD3100. Cells (5 × 10<sup>5</sup> cells/mL) cultured in 6-well plates were treated with 5 and 10 µM AMD3100 and A1, followed by lysis in RIPA buffer supplemented with protease and phosphatase inhibitors. Protein content in the lysates was quantified using Bradford's assay. Subsequently, proteins were separated by SDS-PAGE electrophoresis, transferred onto membranes, and immunoblotted with mouse anti-pAKT antibodies (R&D System, MAB887-SP) along with anti-actin β antibodies (R&D System, MAB8929-SP) for normalization. HRP-conjugated IgG (R&D System, HAF018) was utilized for membrane labeling, and protein bands were visualized through X-ray film exposure. The density and size of the bands were analyzed using Image-J software (version

1.41o, Java 1.6.0\_10, Wayne Rasband, US National Institutes of Health).

**Migration assay**

Migration/Chemotaxis Assay Kit (24-well, 8 μm) (ab235694) was used for migration assay. Initially, CT-26 cells were seeded at a density of 10<sup>6</sup>×5 cells per well and cultured for 24 h in DMEM/F-12 medium under FBS-deprived conditions. Subsequently, 200,000 cells for each counting chamber were treated with 10 μm/mL of AMD3100 and A1 and incubated for 24 h. It is worth mentioning that CXCL12, with a concentration of 300 ng/mL and 600 μL of serum-free DMEM/F-12 medium, was added to the respective lower chambers on the day of the experiment. After a 24 h incubation in a CO<sub>2</sub> incubator, non-migrated cells were removed from the upper compartments using a swab, and migrated cells were stained with 1.0% crystal violet for 30 min at 37 °C and then washed twice with PBS. Finally, after counting the migrated cells in 10 independent microscopic fields, a comparative diagram of the percentage of migrated cells was plotted, and images were captured from the cellular groups.

**Animal model**

This study utilized 36 female BALB/c mice aged 6 to 8 weeks, weighing 15 to 17 g. They were divided into three groups of 12 each and maintained in pathogen-free conditions with proper environmental controls. The Ethics Committee of Iran University of Medical Sciences (IR.IUMS.FMD.REC.1400.590) approved the experimental procedures. The mice were allocated into three groups: Group 1 received PBS (negative control), Group 2 received AMD3100 (drug control), and Group 3 received A1 (case group). Six mice from each group were chosen for further experimentation, while six were monitored for survival analysis. Tumor inoculation was done by injecting 300,000 CT-26 cells subcutaneously into the right flank. Tumor growth was observed, and treatment began on day 13 when tumors reached 150 mm<sup>3</sup>. A 5 mg/kg dose for A1 and AMD3100 was administered intraperitoneally every other day from days 13 to 31 [30–32]. The control group received PBS injections (Fig. 1).

**Evaluation of tregs infiltration**

Following the removal of the tumor tissues, a scalpel was used to cut the tissues into smaller pieces for tumor

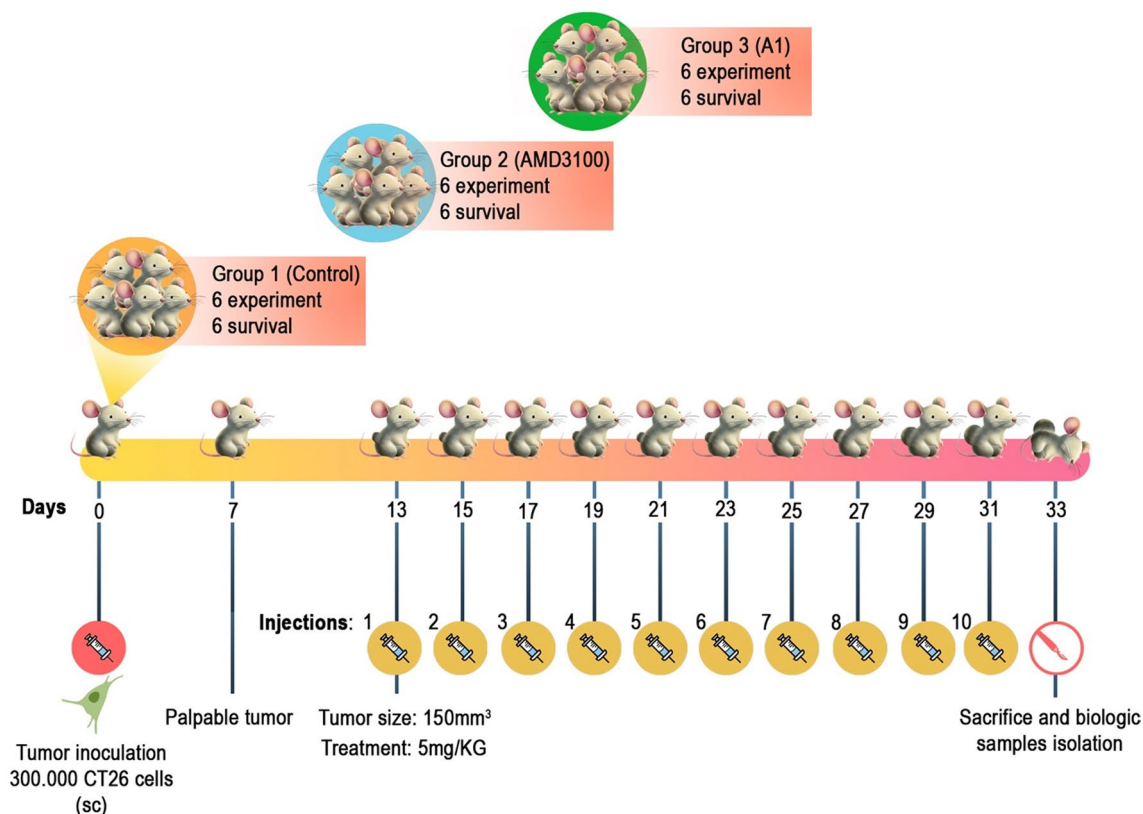


**Fig. 1** An overview of the tumor inoculation and animal treatment protocol. On Day 0, mice were inoculated with tumor cells, subsequently undergoing a treatment regimen over a specified duration. Significant experimental phases are delineated, encompassing inoculation, drug administration, and sample collection

cell dissociation. These pieces were then put in Falcon tubes with a cocktail of DMEM, type IV collagenase enzyme (0.2% concentration) (BIOIDEA, BI-1603, Iran), and DNase type I enzyme (10 units/mL) (Yekta Tajhiz, YT9058, Iran). The tube was incubated for 40 min at 37 °C in a shaker incubator, with regular checks and mixing every 10 min. After the enzymatic digestion, we added a DMEM culture medium containing 10% FBS to block the enzymatic activity. The cell suspension was centrifuged at room temperature for 5 min at 1500×g, and the enzyme-containing supernatant was discarded. The cell suspensions were then passed through a 70 µm cell strainer (SPL, Korea) to remove the possible cell clumps. After centrifuging and washing with PBS, cells were counted and prepared for flow cytometry analysis. For identifying Tregs, fluorophore-conjugated antibodies, including anti-mouse-CD4 (FITC) (100,405), anti-mouse-CD25 (PerCP) (B369413), anti-mouse-FOXP3 (PE) (B383980), and anti-mouse-CD3 (APC) (100,235) (BioLegend, USA) were used for flow cytometry analysis. Supplementary Fig. 3 shows the gating strategy.

#### **Evaluation of CXCR4, VEGF, FGF, IL-10, TGF-β expression at mRNA & protein levels**

Following RNA extraction from the isolated tumor tissues, preserved in RNA Later (KPG, Iran), cDNA synthesis was carried out to assess the expression of target genes, including *VEGF*, *FGF*, *CXCR4*, *IL-10*, and *TGF-β*, with *actin-β* serving as the reference gene by the RT-PCR technique. Tissue concentrations of IL-10 and TGF-β were measured using KPG ELISA kits (KPG, Iran) according to the manufacturer's instructions.

For the immunohistochemistry (IHC) staining of VEGF, we followed the protocol described by Kouvaras et al. [33]. The paraffins were removed, and the tissue sections were rehydrated in water. Natural peroxidase activity was inhibited using a 10% hydrogen peroxide solution for 10 min. Antigen retrieval involved heating the sections at 95 °C in a sodium citrate buffer (10 mM, pH 6) for 30 min. After washing with PBS, the slides were incubated with anti-VEGF primary antibody (R&D Systems, AF767-SP) at 25 °C for 50 min. Following another PBS wash, the secondary antibody was applied at 25 °C for 45 min. Lastly, the sections were counterstained with hematoxylin, covered with diaminobenzidine (DAB) (Thermo Scientific™, 34,002) color-developing solution, and evaluated under a light microscope by an expert pathologist.

#### **Toxicity assay**

Biochemical and histopathological techniques were used to assess the hepatotoxicity of A1 compared to AMD3100 in the treated animals. Serum levels of liver

enzymes, specifically alanine transaminase (ALT) (Delta DP, DDP01154S, Iran) and aspartate transaminase (AST) (Delta DP, DDP01159S, Iran), were measured using a Hitachi-912 autoanalyzer (Hitachi, Mannheim, Germany). Additionally, hematoxylin and eosin (H&E) staining was used to examine the alterations and morphological appearance of the hepatocytes. An expert pathologist screened the slides and subsequently interpreted the resulting microscopic observations.

#### **Statistical analysis**

We used GraphPad Prism version 9 software to analyze the obtained data in this investigation. For normally distributed data, a T-test was employed to compare two groups, while ANOVA tests were utilized to compare multiple groups. In instances of non-normally distributed data, a Mann–Whitney test was applied to compare two groups, and the Kruskal–Wallis test was employed to compare various groups. The presentation of data in this study included Mean ± SD, Mean ± SEM, and the minimum, first quartile, median, third quartile, and maximum values. The significance between the examined groups was determined based on a P-value of less than 0.05. The  $2^{-\Delta\text{Ct}}$  formula was employed to determine the relative expression of the RT-PCR products.

## **Results**

### **Molecular dynamics simulations**

The conformational changes, binding mode interactions, and stability of the target compounds, A1 and AMD3100, and the crystallographic ligand, ITD, and CXCR4 receptor were computed through molecular dynamic simulation studies. The root means square deviations (RMSD) plots confirmed the studied systems' convergence during 100 ns of MDs (Supplementary Information, Figure S4). The per residue root mean square fluctuation (RMSF) values revealed a decreasing trend for CXCR4 in complex with A1 compared to those in complex with ITD, which shows the tighter intercalations of A1 with CXCR4 (Supplementary Information, Figure S5). Further, the target ligands' interactions with the binding groove key residues of CXCR4 were studied according to the MDs studies, confirming the results obtained from the previously performed docking studies (Supplementary Information, Table S1) [17]

The molecular dynamic simulation trajectories of A1/MD3100/ITD-CXCR4 complexes were analyzed to calculate free binding energies. The binding energy of A1 is significantly lower with a reducing trend throughout the MDs studies with the value of  $-50.40 \pm 4.02$  (Kcal / mol) during the last 20 ns of the simulations (Supplementary Information, Table S2, Figure S6, and Figure S7). According to the output of MDs trajectory analysis,

A1 induces more conformational changes to the CXCR4 backbone structure. It establishes stronger interactions, significantly reducing the binding pocket key residue fluctuations.

**CXCR4 expression in MEF & CT-26 Cell Lines**

The results showed that the level of CXCR4 gene expression in CT-26 cells was significantly ( $P=0.005$ ) higher than normal MEF cells by  $4.37 \pm 0.32$  times (Fig. 2A). Correspondingly, the flow cytometry test outcomes showed that the number of CXCR4<sup>+</sup> cells in CT-26 cells was significantly higher than that of MEF ( $P=0.001$ ) (Fig. 2B). These findings confirm the expression of the CXCR4 receptor by CT-26 cells for further analysis.

**Cell proliferation**

The cell proliferation results showed that the concentration of 40 µg/ml A1 and AMD3100 significantly reduced the proliferation ability of CT-26 cells treated with 100 ng/ml CXCL12 in 72 h (Fig. 3). However, this anti-proliferative effect was significant only for the

A1 compared to the CXCL12-stimulated group and untreated control ( $P=0.0134$  and  $P=0.032$ , respectively). Therefore, A1 could effectively inhibit the expansion of CT-26 cells in vitro.

**Functional assays**

The treatment of CT-26 cells with 100 ng/mL CXCL12 for 72 h significantly increased the expression of *CXCR4* ( $P<0.0001$ ), *NFκB* ( $P<0.0001$ ), and *MMP-9* ( $P<0.0001$ ) genes compared to the untreated control group. Whereas, treatment of CT-26 cells with a combination of 60 µg/mL A1 and 100 ng/mL CXCL12 significantly downregulated (inhibited) the gene expression of *CXCR4* ( $P<0.0007$ ), *NFκB* ( $P<0.0001$ ), and *MMP-9* ( $P<0.0001$ ) compared to merely 100 ng/mL CXCL12-treated group (Fig. 4).

The cAMP assay revealed that treatment of the cells with merely 5 µmol/mL forskolin increased the cAMP level by  $135.3 \pm 8.9$  pmol/mL. Whereas treatment of the cells with 5 µmol/mL forskolin and 100 ng/mL CXCL12 resulted in significantly lower cAMP

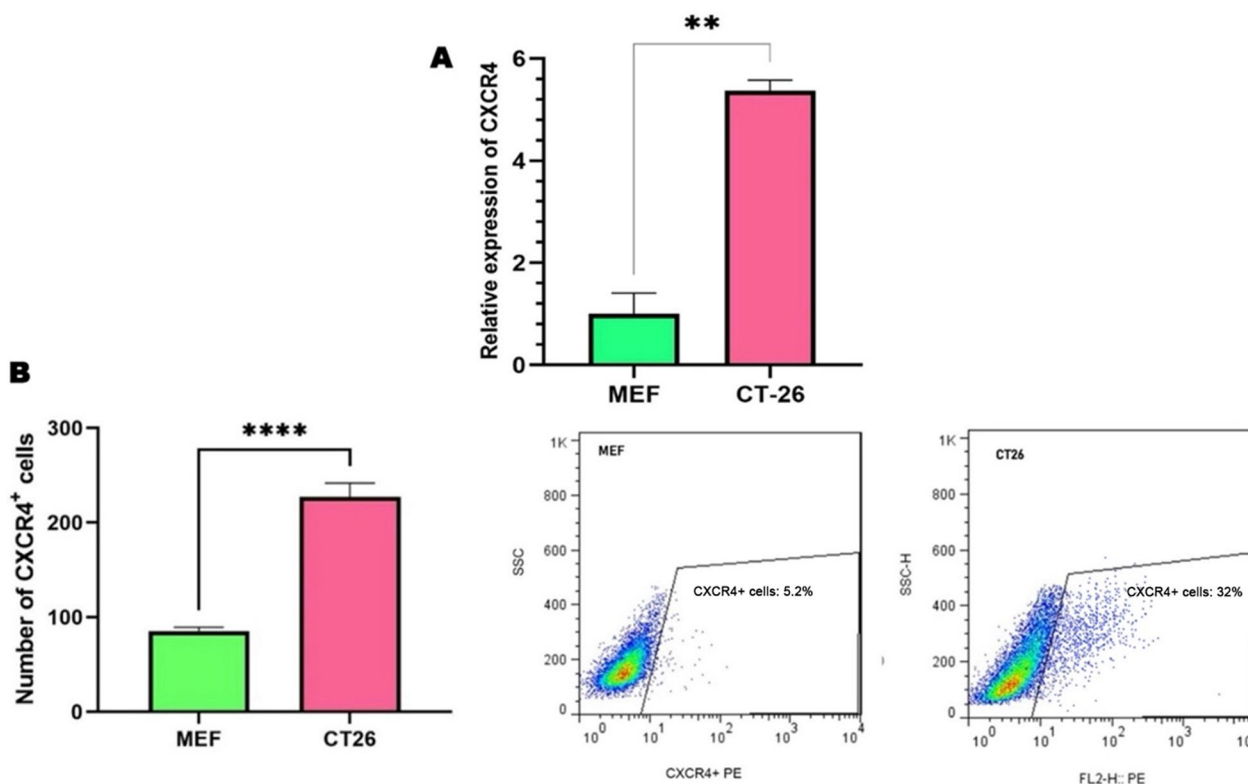


**Fig. 2** CXCR4 expression in MEF and CT26 cell lines. (A) The bar graph illustrates the relative gene expression levels of CXCR4 in CT26 and MEF cell lines. (B) The bar graph represents the quantity of CXCR4-positive cells within CT26 and MEF cell populations, as quantified by flow cytometry. Below, the bar graph shows representative flow cytometry dot plots, showcasing the percentage of CXCR4-positive cells in each cell line (5.2% for MEF and 32% for CT26). The experiments were performed in triplicate. The results are expressed as the mean ± standard deviation (SD) from three independent experiments, with \*\* denoting statistical significance at  $P < 0.01$  and \*\*\*\* indicating a statistical significance level of  $P < 0.0001$

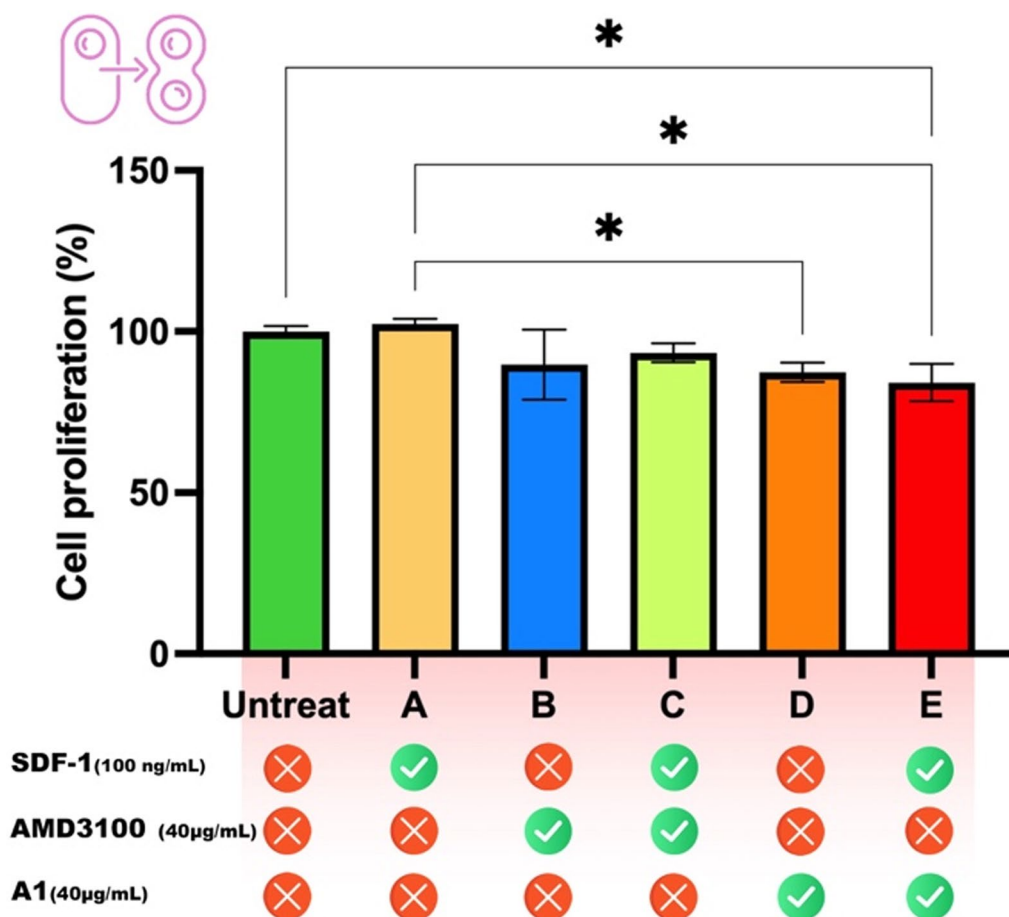


**Fig. 3** The bar graph illustrates the percentage of cell proliferation across various treatment conditions, utilizing the untreated group as the baseline (100%) for comparative analysis. Groups A through E signify different treatment combinations: Group A received SDF-1 (100 ng/mL), Group B was administered AMD3100 (40 µg/mL), Group C was subjected to both SDF-1 (100 ng/mL) and AMD3100 (40 µg/mL), Group D received A1 (40 µg/mL), and Group E was treated with the combination of SDF-1 (100 ng/mL) and A1 (40 µg/mL). Statistical analysis indicated that the untreated group exhibited significantly higher cell proliferation than Group B (\*p < 0.05). Group A, treated exclusively with SDF-1, demonstrated significantly elevated cell proliferation relative to Groups B, D, and E (\*p < 0.05). Conversely, no significant differences were detected among Groups C, D, and E. The statistical evaluations were performed using one-way ANOVA followed by post-hoc analysis, with asterisks denoting substantial differences (\*p < 0.05). The error bars represent three independent experiments' standard deviation (SD). These findings imply that SDF-1 alone (Group A) results in the highest cell proliferation, while A1 and AMD3100 attenuate this effect. SDF-1; stromal-derived factor 1 (CXCL12)

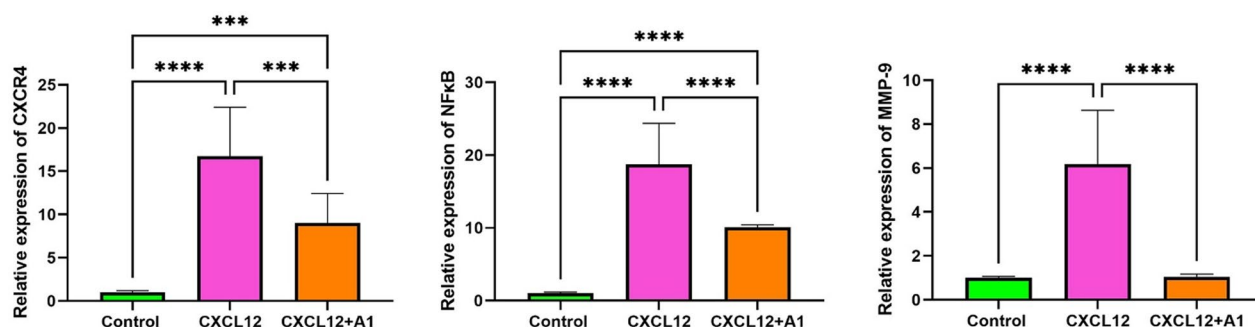


**Fig. 4** Comparative CXCR4, NFκB, and MMP-9 gene expression levels across CT-26 untreated and treated cells. The accompanying graph illustrates the relative gene expression levels in cells subjected to treatment with CXCL12 either alone or in combination with A1. The data is represented as Mean ± SD derived from three independent experiments. Significance levels are indicated with \*\*\*\* for P < 0.0001 and \*\*\* for P < 0.001, demonstrating the statistical differences among the treatment groups

level ( $37.47 \pm 11.8$  pmol/mL) ( $P=0.0001$ ) (control group). Meanwhile, cells treated with 100 nmol/mL of A1, along with 5  $\mu$ mol/mL forskolin and 100 ng/mL CXCL12, showed significantly higher cAMP levels ( $85.94 \pm 37.14$  pmol/mL) compared to the control group ( $P=0.0255$ ). Additionally, AMD3100 at a concentration of 1000 nmol/mL could increase the cAMP level by  $86.96 \pm 15.9$  pmol/mL, which was statistically significant compared to the control group ( $P=0.0222$ ). However, the most significant effect was associated with the concentration of 1000 nmol/mL of A1, which, together with 5  $\mu$ mol/mL forskolin and 100 ng/mL CXCL12, could increase the level of cAMP by  $120.5 \pm 3.36$  pmol/

mL, which in comparison to the control group was significantly higher ( $P=0.0003$ ) (Fig. 5).

The findings indicated that both AMD3100 and A1 suppress CXCL12-induced AKT phosphorylation in a dose-dependent manner. Western blot examination indicated a discernible decrease in pAKT levels when the concentration of AMD3100 or A1 escalates from 0 to 10  $\mu$ M, while Actin- $\beta$  levels stay stable (Fig. 6A). The quantification of these data indicated that in cells treated with AMD3100, pAKT expression considerably reduced at 10  $\mu$ M compared to both the control ( $p<0.001$ ) and 5  $\mu$ M groups ( $p<0.01$ ). Nonetheless, no substantial change is seen between the control and 5  $\mu$ M doses (Figs. 6B and C). A1 therapy significantly decreases

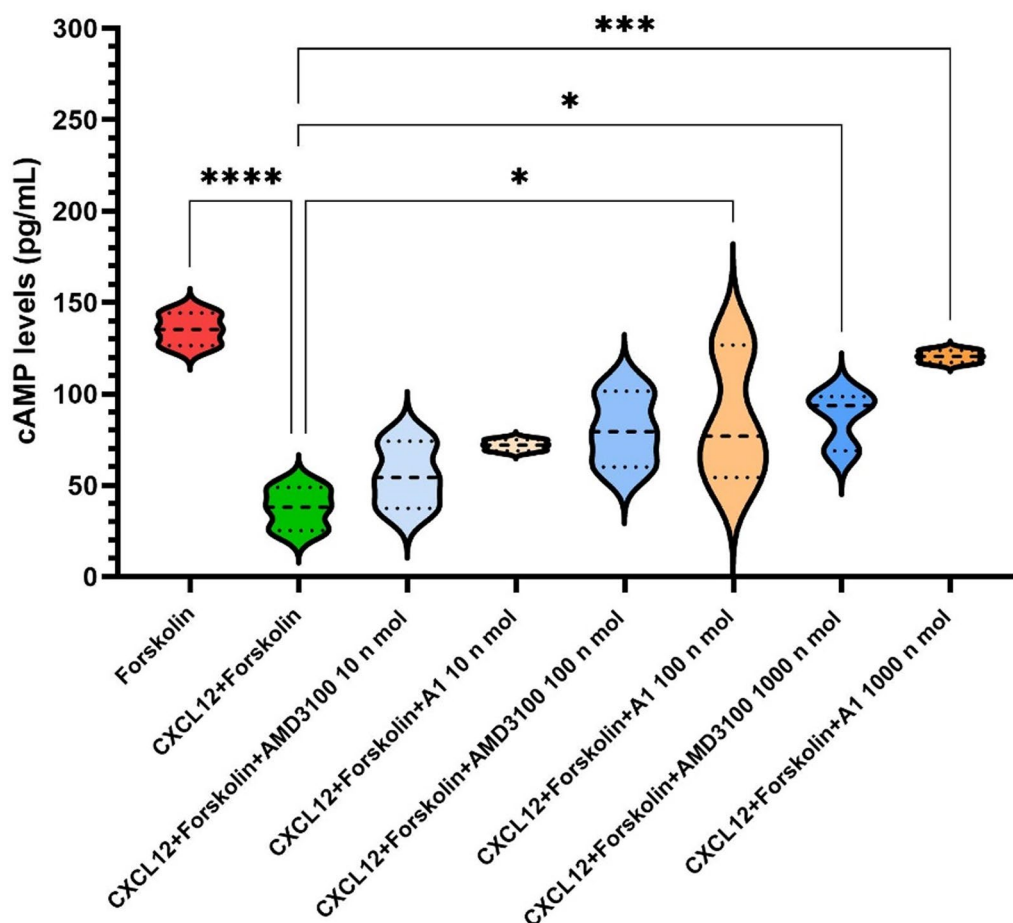


**Fig. 5** Comparative analysis of intracellular cAMP levels in response to forskolin, CXCL12, and varying concentrations of A1 and AMD3100 in CT-26 cells. The graph illustrates cellular levels of cAMP in response to treatment with forskolin, CXCL12, and increasing doses (10 nmol/ml, 100 nmol/ml, and 1000 nmol/ml) of A1 and AMD3100. The experiments were conducted in triplicate, and the data are represented utilizing box-and-whisker plots, which display the minimum, first quartile, median, third quartile, and maximum values. The treatment with forskolin is a positive control to validate the cAMP assay, while CXCL12 functions as the physiological stimulus. Significant reductions or elevations in cAMP levels resulting from drug treatments are indicated. Statistical analysis was executed using ANOVA, with significance levels: \* $P < 0.05$ , \*\*\* $P < 0.001$ , and \*\*\*\* $P < 0.0001$ , indicating varying degrees of significance between the control and treated groups. Error bars represent the variability observed across experimental replicates

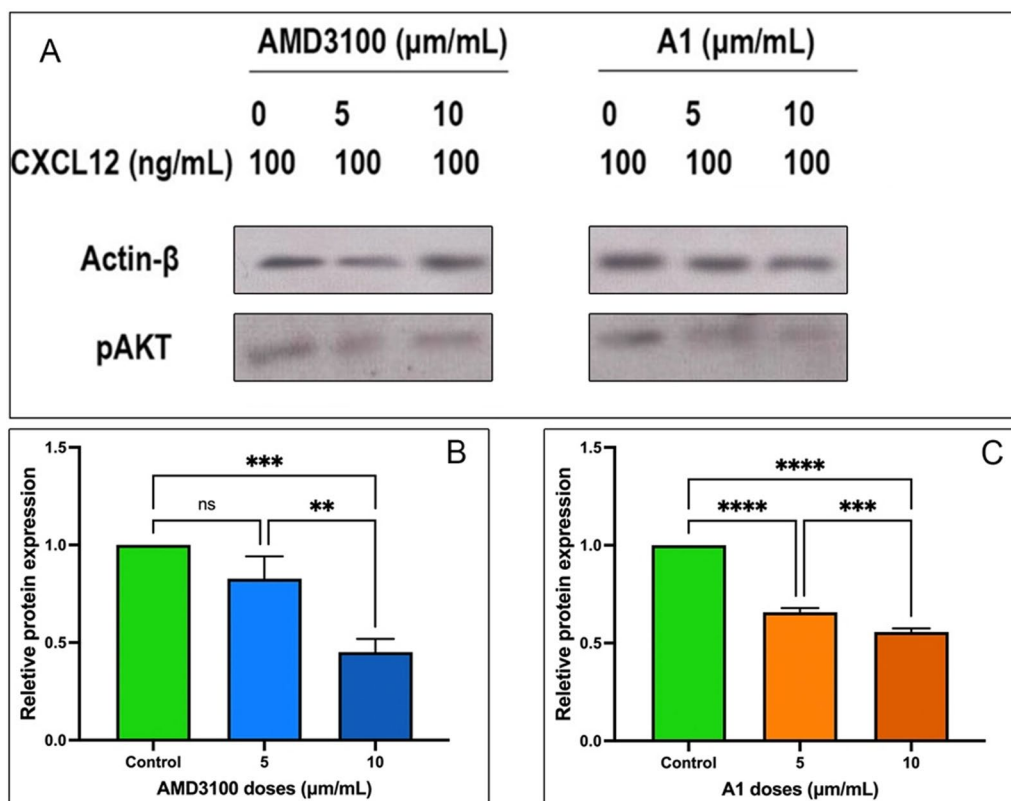


**Fig. 6** The figure illustrates the inhibitory effects of AMD3100 and A1 on CXCL12-induced AKT phosphorylation in CT-26 treated cells. In panel (A), representative Western blot images depict the expression of phosphorylated AKT (pAKT) and Actin-β (as a loading control) in cells subjected to 100 ng/mL of CXCL12 alongside increasing concentrations of either AMD3100 or A1 (0, 5, and 10 μM). The treatment with AMD3100 and A1 resulted in a noticeable reduction in pAKT levels compared to the control group. Panels (B) and (C) quantify the relative pAKT expression normalized to Actin-β for AMD3100 and A1, respectively. In panel (B), cells treated with 10 μM AMD3100 exhibited a statistically significant decrease in pAKT levels compared to both the control (\*\*\* $p < 0.001$ ) and the 5 μM groups (\*\* $p < 0.01$ ). Conversely, the difference between the control and the 5 μM groups was not statistically significant. In panel (C), A1 treatment demonstrated a significant reduction in pAKT levels in both the 5 μM (\*\*\*\* $p < 0.0001$ ) and 10 μM (\*\*\* $p < 0.001$ ) groups in comparison to the control, with the 10 μM group exhibiting a further reduction relative to the 5 μM group (\*\*\*\* $p < 0.0001$ ). Statistical analysis was performed utilizing one-way ANOVA followed by Tukey's post hoc test, and the data are presented as mean ± SEM from three independent experiments

pAKT at both 5 μM ( $p < 0.0001$ ) and 10 μM ( $p < 0.001$ ) relative to the control group. Moreover, pAKT levels are markedly reduced in the 10 μM A1 group relative to the 5 μM group ( $p < 0.0001$ ), indicating a more pronounced inhibitory impact at higher dosages. The results demonstrate that AMD3100 and A1 efficiently inhibit CXCL12-induced AKT activation, with A1 exhibiting a more significant effect across various doses. Moreover, flow cytometry analysis of the CXCR4 receptor expression on CT-26 cells showed that the treatment of CT-26 cells with 60 μg/mL A1 along with 100 ng/mL CXCL12 for 72 h significantly reduced CXCR4<sup>+</sup> cell count compared to the merely 100 ng/mL CXCL12-treated control group ( $P < 0.0001$ ) (Fig. 7).

Collectively, the findings obtained from functional assays can confirm A1's inhibitory function on the CXCR4 receptor and its downstream signaling pathways.

#### Migration assay

The effect of different doses of A1 and AMD3100 on the migration of CT-26 cells was investigated, and the final dose was 10 μmol/mL for both compounds. As shown in Fig. 8, the percentage of migrating CT-26 cells after treatment with 300 ng/mL CXCL12 increased significantly compared to the untreated group ( $p = 0.0306$ ), which indicates the stimulatory effect of CXCL12 on the CXCR4 receptor and its downstream pathways, which ultimately leads to locomotion and cell migration. Moreover, the percentage of migrating CT-26 cells following the treatment of cells with 10 μmol/mL of both A1 ( $P < 0.001$ ) and AMD3100 ( $P < 0.05$ ) was significantly lower than the control group (treated with 300 ng/ml CXCL12). However, this reduction was more remarkable for the AMD3100. Hence, both AMD3100 and A1 can diminish the migration of CT-26 cells by inhibiting CXCR4.

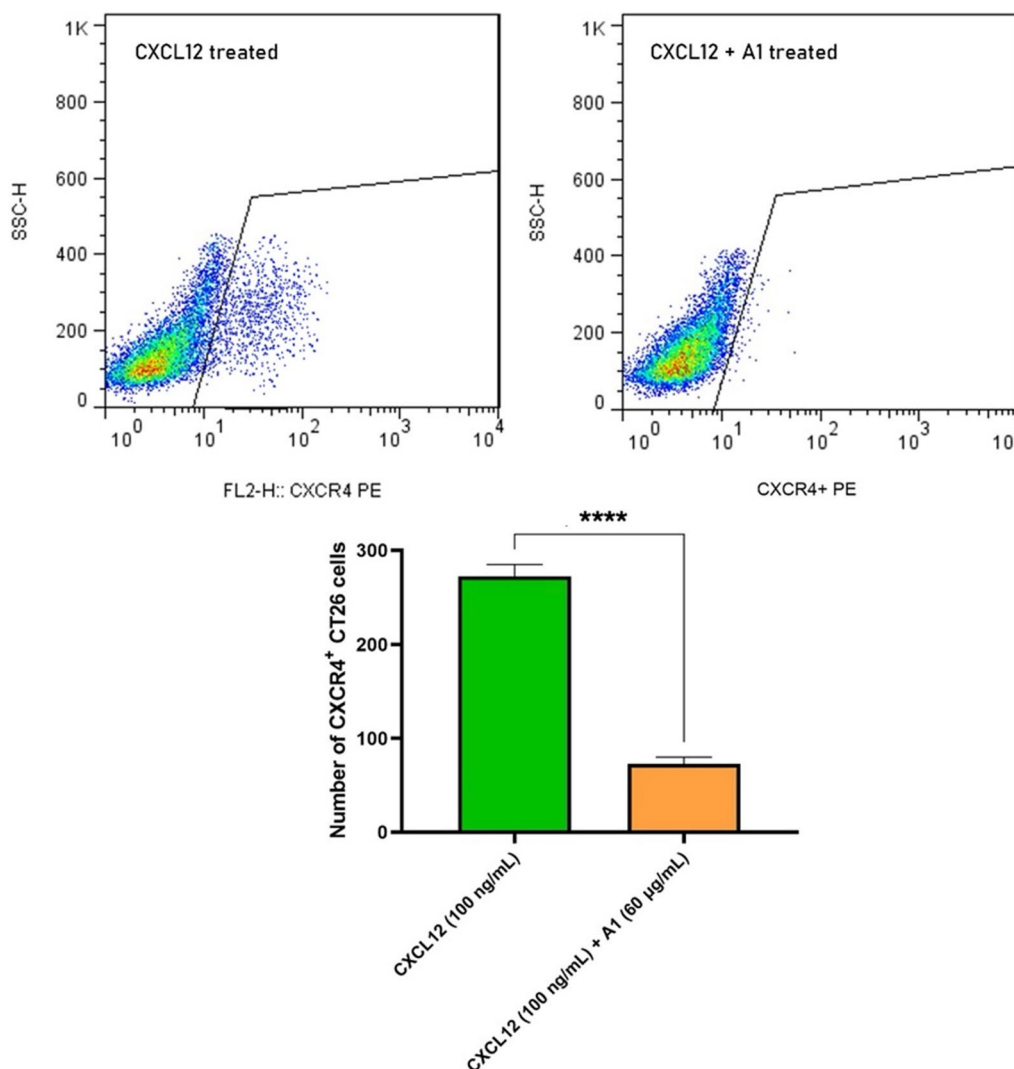


**Fig. 7** Comparative analysis of the effect of 60 µg/ml A1 on the number of CXCR4<sup>+</sup> CT-26 cells compared to treatment with 100 ng/ml CXCL12. This graph illustrates the alterations in the number of CXCR4<sup>+</sup> expressing cells in response to a dosage of 60 µg/ml of drug A1 in comparison to cells treated with 100 ng/ml of CXCL12, which is a recognized chemokine ligand for CXCR4. The experiments were conducted in triplicate, and the data are presented as Mean ± SD. The treatment groups are evaluated to assess the relative impact of A1 on the CXCR4<sup>+</sup> cell populations in contrast to the stimulation induced by CXCL12. Statistical significance is denoted by \*\*\*\*P < 0.0001, indicating a highly significant difference between the treated groups. The error bars represent the standard deviation among replicates, ensuring the experimental results' reproducibility

**Treg infiltration in the TME and spleen**

One of the goals of inhibiting the CXCR4 receptor in cancer treatment approaches is to reduce the migration and infiltration of immune cells with a regulatory and tumor-supporting phenotype in the TME. Among the most prominent of these cells are Tregs with the usual CD3<sup>+</sup>CD4<sup>+</sup>CD25<sup>+</sup>FOXP3<sup>+</sup> phenotype, which inactivates anti-tumor immune responses by secreting immune system inhibitory cytokines such as IL-10 and TGF-β. In this study, we investigated the percentage of regulatory T cells in the TME and spleen by flow cytometry. The results showed that the percentage

of Tregs in the tumor tissue of mice treated with AMD3100 (P = 0.0006) and A1 (P = 0.0069) was significantly lower than the control group (Fig. 9A).

Examining the spleen tissue cells showed a significantly lower percentage of Tregs in mice treated with AMD3100 (P < 0.0001) and A1 (P < 0.0001) compared to the control group. We found that AMD3100 works better than A1. The difference between AMD3100 and A1 was also significant in this test (P = 0.0009) (Fig. 9B). These findings demonstrate that inhibiting CXCR4 by A1 and AMD3100 can effectively manage both local and systemic immunosuppressive responses

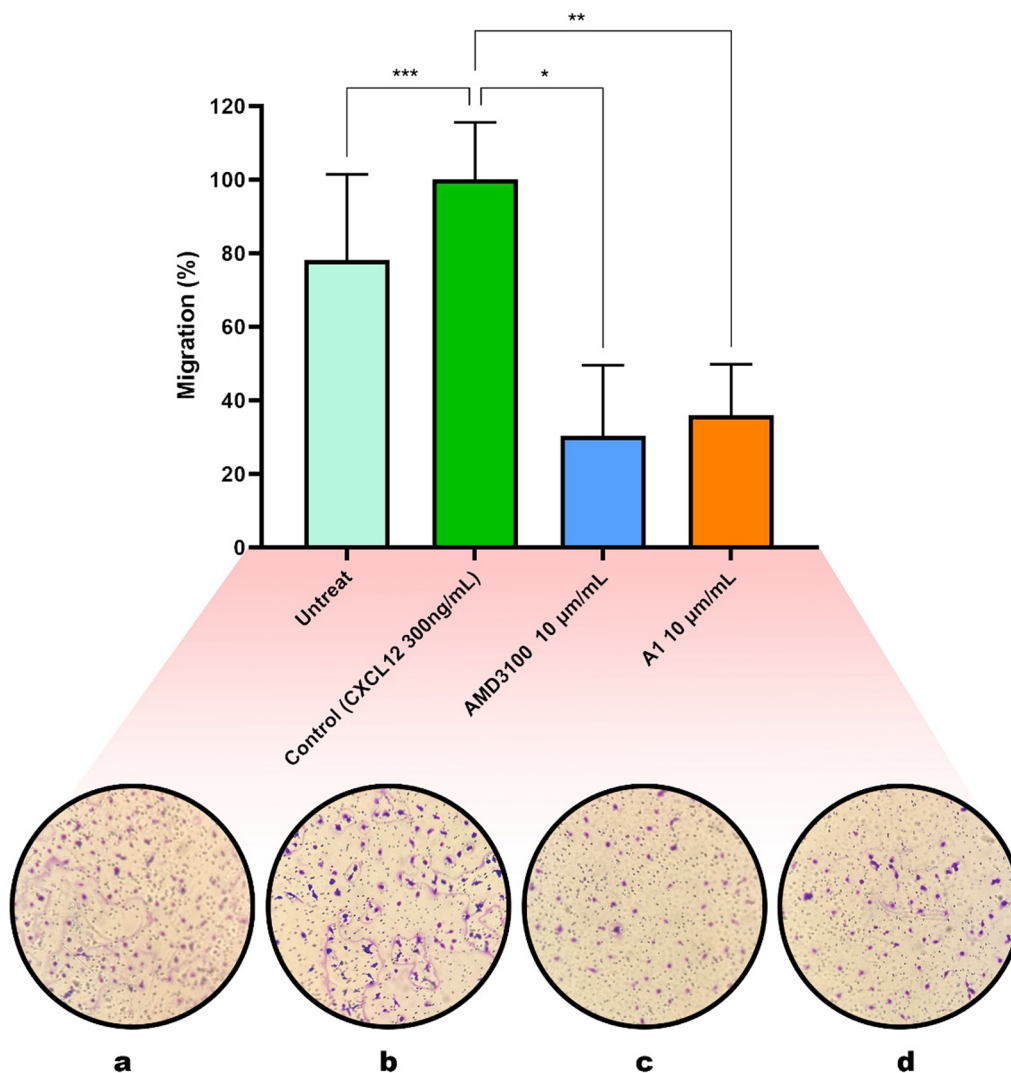


**Fig. 8** CT-26 cell migration analysis after treatment with CXCL12, A1, and AMD3100. The graph illustrates the percentage of migrating CT-26 cells following exposure to 300 ng/ml CXCL12, 10 µm/ml A1, and 10 mM/ml AMD3100. Four experimental conditions are represented: **(a)** untreated cells (baseline migration), **(b)** cells treated with CXCL12 (control group to induce migration), **(c)** cells treated with AMD3100 (CXCR4 antagonist), and **(d)** cells treated with A1 (experimental drug). The results are expressed as mean  $\pm$  SD from triplicate experiments. Statistical significance is indicated as follows: \* $P < 0.05$ , \*\* $P < 0.01$ , and \*\*\* $P < 0.001$ , reflecting varying degrees of significance compared to the control group treated with CXCL12. These findings emphasize the effects of A1 and AMD3100 on the migratory behavior of CT-26 cells in response to chemotactic stimulation by CXCL12. Error bars denote the standard deviation between replicate experiments, ensuring the data's reliability

by decreasing the frequency of Treg infiltration in the CRC model.

#### Angiogenic and immunosuppressive gene expression in the TME

The expression level of the *CXCR4* gene in the groups treated with A1 was  $0.26 \pm 0.44$ -fold, and in the AMD3100-treated group was  $0.427 \pm 0.39$ -fold, indicating lower results than the control group ( $0.86 \pm 1$ ). However, this decrease was not statistically significant (Fig. 10A). According to the role of growth factors in

angiogenesis and tumor mass growth, *FGF* and *VEGF* genes were investigated in BALB/c mice treated with A1 and AMD3100 tumor tissue. The results showed that the expression of the *FGF* gene in A1-treated groups was  $1.56 \pm 1.7$ -fold, and in the AMD3100-treated group, it was  $3.55 \pm 2.04$ -fold, showing a higher expression rate than the control group ( $0.56 \pm 1$ ); however, this difference was not statistically significant (Fig. 10B). Regarding the *VEGF* gene, the results were in an opposite condition, so in A1-treated groups, the relative expression rate was  $0.1 \pm 0.03$ -fold. The

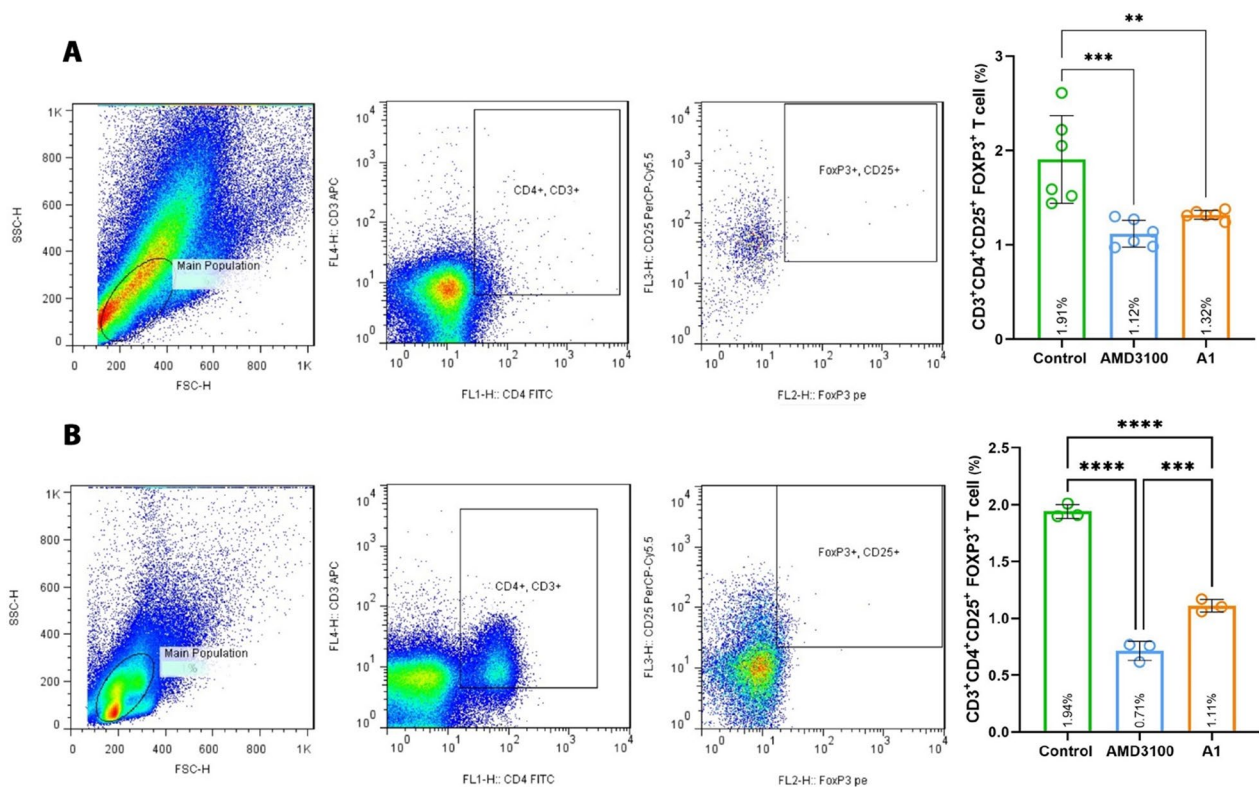


**Fig. 9** Flow cytometry analysis of Treg distribution in the TME and spleen of treated mice. The diagrams illustrate the percentage of T regulatory cells (Tregs) in the (A) tumor microenvironment (TME) and (B) spleen of mice administered with the pharmacological agents A1 and AMD3100, as compared to untreated control groups. Flow cytometry was utilized to evaluate Treg populations, employing specific gating strategies to identify CD4<sup>+</sup>CD25<sup>+</sup>FoxP3<sup>+</sup> cells. The experiments were triplicate, with data presented as Mean  $\pm$  Standard Deviation (SD). Statistical significance is denoted by \*\* $P < 0.01$  and \*\*\* $P < 0.001$ , highlighting the variations in Treg distribution between treatment and control groups. These findings demonstrate the influence of A1 and AMD3100 on the modulation of the immune landscape within the TME and systemic lymphoid organs. Error bars represent the standard deviation among replicate experiments, ensuring consistency and reproducibility of the data

AMD3100-treated group was  $0.23 \pm 0.29$ -fold, indicating a lower expression level than the control group ( $1.23 \pm$  onefold). This difference between the groups was statistically significant only between those treated with A1 compared to the control group ( $P = 0.05$ ) (Fig. 10C). Regarding *IL-10* gene expression, both compounds provided almost the same effect in reducing its expression level (Fig. 10D). The results showed that the expression of *IL-10* gene in the A1-treated groups was  $0.24 \pm 0.05$ -fold. In AMD3100-treated groups, it was  $0.24 \pm 0.15$ -fold, showing lower results than the control group ( $0.4 \pm$  onefold), and the difference between the groups treated with compounds compared to the control group was statistically significant ( $P = 0.007$ ). Moreover, the findings showed that both compounds, especially A1, could prevent *TGF- $\beta$*  gene expression. So, the A1-treated group showed  $0.004 \pm 0.001$ -fold expression ( $P = 0.013$ ), and the AMD3100-treated group revealed  $0.01 \pm 0.006$ -fold expression ( $P = 0.012$ ),

showing significantly much lower expression level than the control group ( $1 \pm 0.6$ -fold) (Fig. 10E).

#### Tumor tissue cytokine & VEGF Levels

The results of the analysis of tissue cytokine concentrations in the TME of BALB/c mice treated with A1 and AMD3100 compounds showed that the tissue levels of TGF- $\beta$  in tumor tissue of mice treated with A1 decreased by  $761.2 \pm 141.8$  pg/mL compared to the AMD3100 group ( $924.2 \pm 811.2$  pg/mL) and control ( $1494 \pm 755.3$  pg/mL). However, this decrease was not statistically significant (Fig. 11A). In addition, tissue levels of IL-10 in mice treated with A1 were  $6350 \pm 546.9$  pg/mL compared to the AMD3100 group ( $264.6 \pm 6435$  pg/mL) and the control group ( $6517 \pm 579.6$  pg/mL) had a decrease. However, this decrease was not statistically significant. These results show that the A1 compound, in addition to inhibiting the expression of genes related to inhibitory cytokines and the infiltration of Tregs, can also reduce

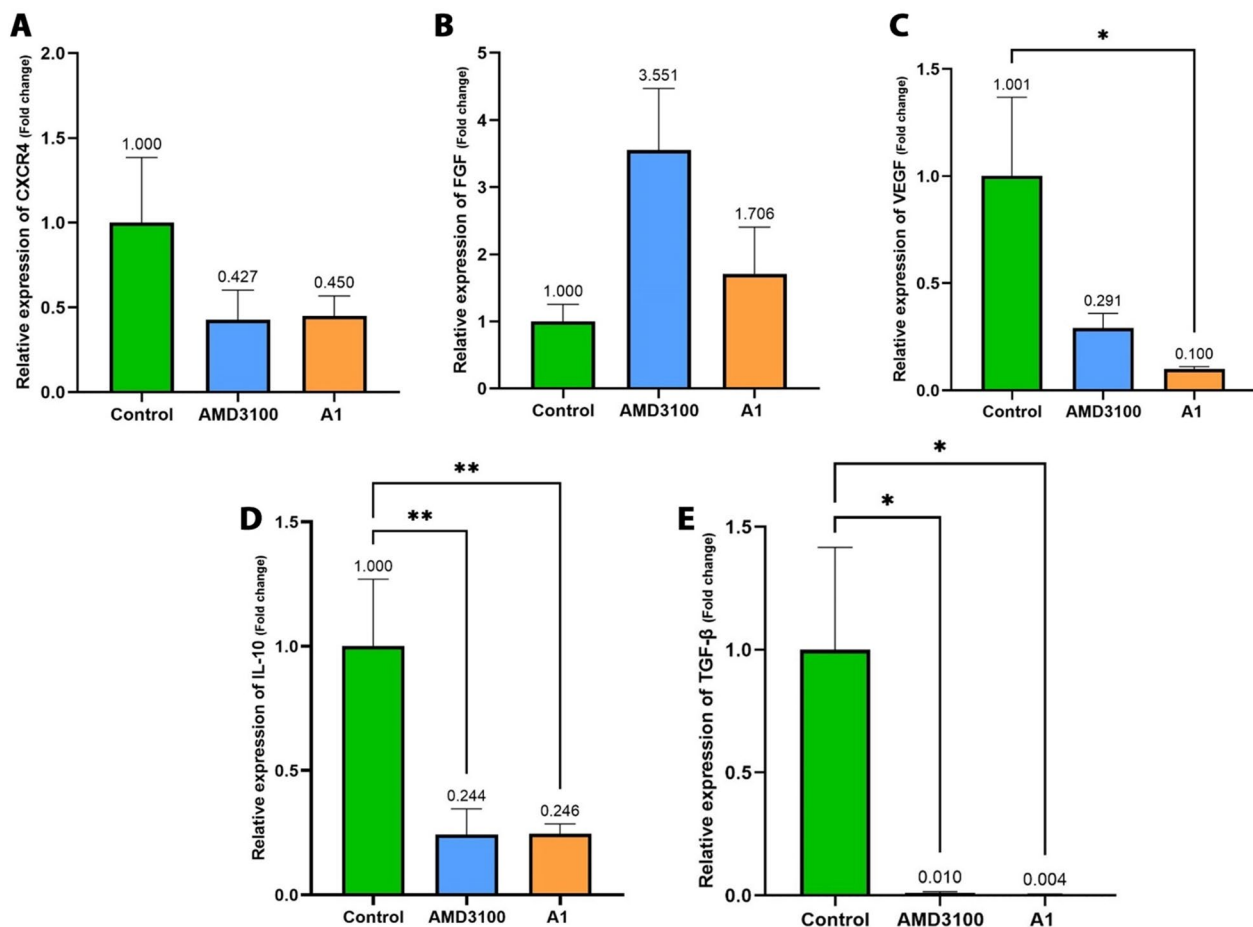


**Fig. 10** Comparative analysis of gene expression levels in tumor tissues of control, AMD3100, and A1-treated mice. The chart illustrates the relative expression levels of (A) *CXCR4*, (B) *FGF*, (C) *VEGF*, (D) *IL-10*, and (E) *TGF-β* genes within tumor tissues derived from three distinct groups: the control group (untreated), the AMD3100-treated group, and the A1-treated group of mice. Gene expression levels were quantified using qRT-PCR, and all experiments were performed in triplicate. The data is presented as Mean ± SEM, reflecting the variability among biological replicates. Statistical significance between the groups is denoted by \* $P < 0.05$  and \*\* $P < 0.01$ , underscoring the differential expression of genes induced by AMD3100 and A1 treatments compared to the control group. These findings elucidate the modulatory effects of the treatments on critical genes implicated in tumor progression, angiogenesis, and immune regulation. Error bars reflect the standard error of the mean, thereby highlighting the consistency of the experimental outcomes

the function of these cells in the TME (Fig. 11B). According to the semi-quantitative results of the IHC, the intensity score of VEGF tissue expression in A1-treated mice was significantly lower than in the control group ( $P = 0.034$ ) (Fig. 12).

These outcomes indicate that inhibition of CXCR4 by A1 can effectively suppress VEGF-mediated angiogenesis and reduce the expression of IL-10 and TGF-β as tumor-supportive cytokines at mRNA and protein levels.

**Tumor size, tumor size, body weight, and survival rate**

According to various studies and ethical guidelines, the subcutaneous tumor size in BALB/c mice should not exceed 15–20 mm in diameter or 1800–2500 mm<sup>3</sup> in

total volume [34]. In the present study, the minimum tumor size was considered to sacrifice the mice to prevent excessive pain and damage to the mice. The weight of mice was measured and recorded using a digital caliper every two days from day 0 to day 33. The results showed that the difference in tumor size in the control, AMD3100, and A1 groups became significant ( $p < 0.0001$ ) (Fig. 13 A). The average tumor size in the control group on the last day of treatment (day 33) was 207.9 ± 93 mm<sup>3</sup>. The tumor size on the same day in the AMD3100 and A1 groups was 691.69 ± 5.67 and 435.6 ± 81.47 mm<sup>3</sup>, respectively (Fig. 13 A).

The results showed a significant reduction in tumor weight in the A1-treated and AMD3100-treated groups

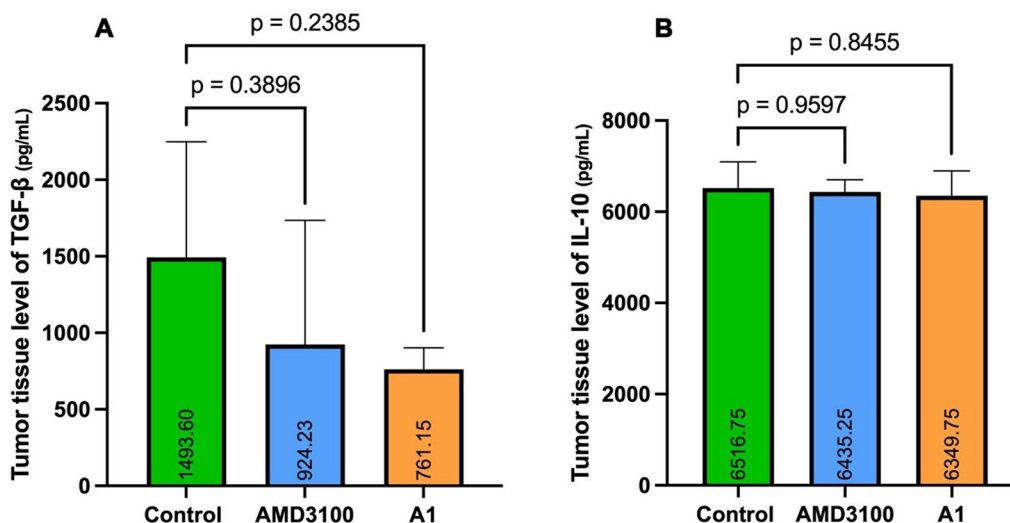


**Fig. 11** Comparative analysis of TGF-β and IL-10 protein expression in the TME of control, AMD3100, and A1-treated mice. The graph illustrates the tissue expression levels of (A) TGF-β and (B) IL-10 proteins within the TME across three experimental groups: control (untreated), AMD3100-treated, and A1-treated mice. Protein expression was quantified using immunohistochemistry or an equivalent technique, and the experiments were duplicated. The data are presented as Mean ± Standard Deviation (SD), emphasizing sample variability. This analysis elucidates the effects of AMD3100 and A1 on the expression of immunosuppressive proteins within the TME, which play pivotal roles in tumor progression and immune evasion. The error bars denote the standard deviation, underscoring the precision and reproducibility of the results

compared to the control group. Tumor weights in the A1 group were significantly lower (~1 g) than in the control (~3.9 g,  $p < 0.0001$ ) and AMD3100 (~2.2 g,  $p < 0.001$ ) groups. There was no significant difference between the A1 and AMD3100 groups, though A1 treatment substantially reduced tumor weight (Fig. 13B). There is no significant difference regarding animal weight between the control, AMD3100, and A1 groups. The average weight on day 0 of the study was  $15.55 \pm 0.75$  g in the control group,  $15.52 \pm 0.29$  g in the AMD3100 group, and  $15.78 \pm 0.81$  g in the A1 group. These values on the last day of the study (day 33) were  $24.85 \pm 8.44$  g,  $22.26 \pm 5.95$  g, and  $20.91 \pm 5.88$  g for the control, AMD3100, and A1 groups, respectively (Fig. 13C).

Kaplan–Meier survival curve and Log-rank test were used to check the survival of treated and control mice after tumor induction (Fig. 13D). In this study, on the 13th day, the average tumor size in three groups was between 150 and 200 mm<sup>3</sup>, which is acceptable for starting animal treatment. After ten injections every other day, on the 33rd day, the mice of the experimental group in all three groups were sacrificed, and their biological samples were separated and stored in accordance with the ethical principles related to laboratory animals. The mice of the survival group were also kept under suitable conditions, and the occurrence of death or survival was recorded daily. Mice with a tumor size of more than 1500 mm<sup>3</sup> were recorded as death events

and euthanized by CO<sub>2</sub> gas due to ethical issues. The results showed that until the 40th day after tumor induction, all mice in the control group gradually died or their tumor size exceeded the mentioned amount. All six mice in the group treated with AMD3100 died or increased tumor size until the 52nd day after tumor induction and were removed from the study. Four out of six mice treated with the A1 compound were removed due to the increase in tumor size, and two mice in this group survived until the 60th day after tumor induction, but based on recent studies and regulations. Due to the tumor size reaching 1500 mm<sup>3</sup>, the mice were excluded from the study in compliance with ethical principles, and the 60th day was considered the end of the survival study [35]. The Log-rank test results showed that the difference in survival percentage between the three groups is significant ( $P < 0.0001$ ). To further investigate all two-group modes, including control with AMD3100 ( $P = 0.0011$ ), control with A1 ( $P = 0.0005$ ), and A1 with AMD3100 ( $P < 0.043$ ) statistically and the percentage of survival were compared. There was a significant difference in all three cases. The median survival value for the control group was 36.5, the AMD3100 group was 47.5, and the A1 group was 53.5 days.

Hence, both A1 and AMD3100 inhibit CXCR4, reducing tumor size and extending survival rates among the studied animals. However, A1 exhibits greater effectiveness in these instances.

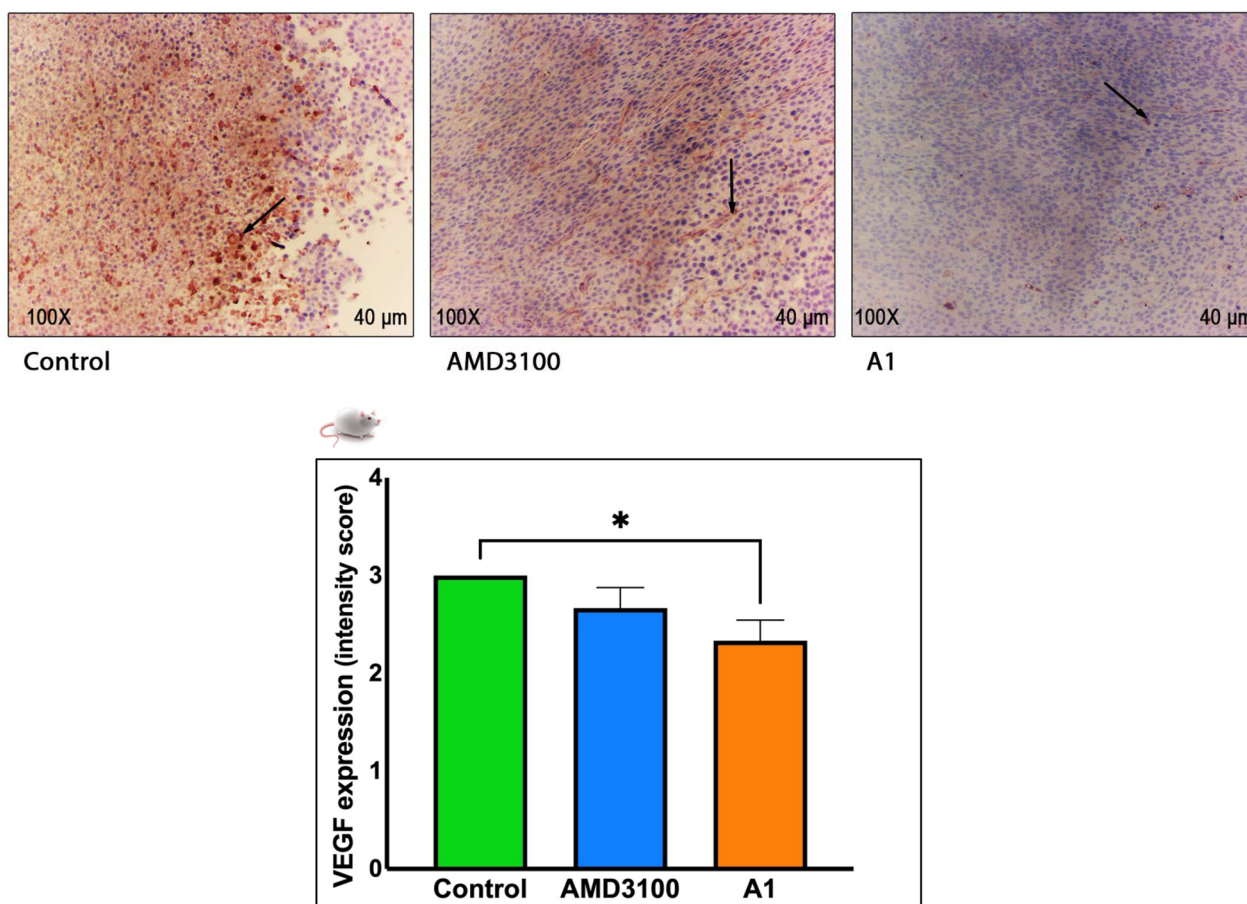


**Fig. 12** Immunohistochemical analysis of VEGF expression in tumor tissues on day 33 post-inoculation in control, AMD3100-treated, and A1-treated mice. Representative images illustrate the expression of Vascular Endothelial Growth Factor (VEGF) in control groups treated with phosphate-buffered saline (PBS), as well as in groups treated with AMD3100 and A1. Immunohistochemical staining was conducted at a magnification of 100X, accompanied by a scale bar of 40 μm. The assessment of VEGF expression was executed semi-quantitatively, utilizing an intensity scoring system, with the corresponding graph providing a comparative analysis of VEGF staining intensity across the various treatment groups. All experiments were performed in triplicate, and the resulting data are presented as Mean ± Standard Deviation (SD). Statistical significance has been indicated by \*P < 0.05, highlighting significant differences in VEGF expression between the control and treatment groups. This analysis elucidates the impact of AMD3100 and A1 on the expression of angiogenic factors within tumor tissues, which may influence tumor growth and vascularization

### Liver toxicity assays

The results showed that in rats receiving 5 mg/Kg of A1 compound, the serum level of ALT enzyme was  $37.33 \pm 32.93$  IU/mL, which compared to the control group receiving PBS ( $21.03 \pm 33.76$  IU/ml) did not change significantly. In the group of animals receiving the AMD3100 compound, the ALT enzyme serum level increased to  $75.67 \pm 11.55$  IU/mL, which was not statistically significant compared to the control group (Fig. 14A). Furthermore, regarding liver enzyme AST, the results showed that in BALB/c mice receiving 5 mg/Kg of compound A1, the serum level of AST enzyme was  $24.15 \pm 15.39$  IU/mL, which compared with the control group receiving placebo ( $16.23 \pm 2.12$  IU/mL) did not

change significantly. In contrast, in the group of animals receiving the AMD3100 drug, the ALT enzyme serum level increased to  $203.07 \pm 54.86$  IU/mL, which was statistically significant compared to the control group (Fig. 14B).

The histopathological findings showed that in the control group, the status of hepatocytes, portal and vascular space, and interstitial tissue were close to normal, and there were no prominent pathological findings. Hepatocyte degeneration was also negative. In the group treated with AMD100, there were inflammatory lesions with infiltration of mononuclear inflammatory cells around the portal space and the vessels. However, no fibrosis was observed in the liver, and hepatocytic degeneration was

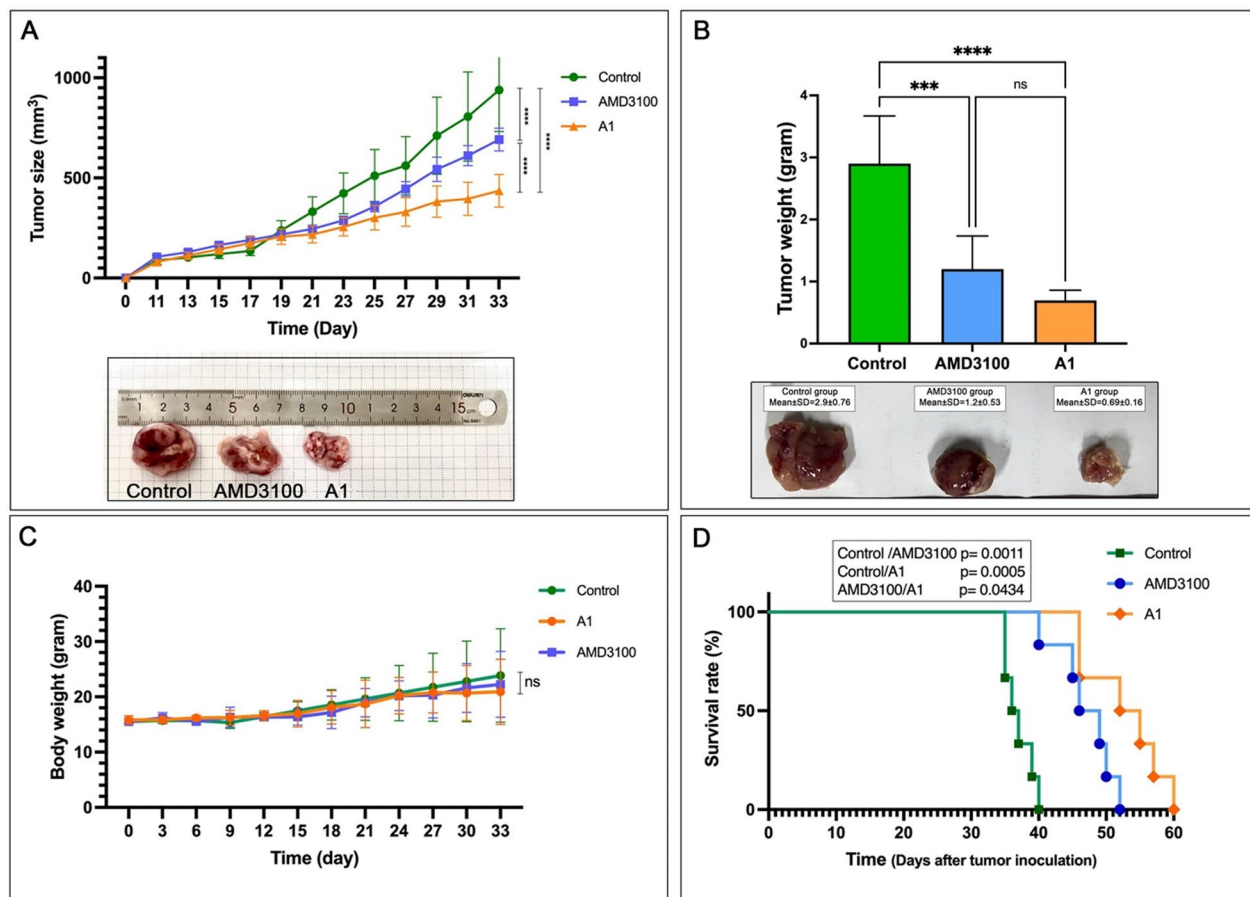


**Fig. 13** (A) Tumor size growth curve over time (days) for three experimental groups: Control (green), AMD3100 treatment (blue), and A1 treatment (orange). Tumor sizes were measured in cubic millimeters (mm<sup>3</sup>) every 2–4 days for 33 days post-tumor inoculation. The A1-treated group showed significantly reduced tumor growth compared to the Control and AMD3100 groups. The inset at the bottom shows representative tumor images from each group after dissection. Data are presented as mean ± SD, \*\*\**p* < 0.001, \*\*\*\**p* < 0.0001. (B) Tumor weight comparison between the Control, AMD3100, and A1 groups. Tumors were weighed post-sacrifice at the end of the experiment. A1 treatment resulted in a significant reduction in tumor weight compared to both the Control and AMD3100 groups. Data are shown as mean ± SD. Statistical significance is indicated by \*\*\**p* < 0.001 and \*\*\*\**p* < 0.0001. Below the graph are images of representative tumors from each group. (C) Body weight progression of mice over the experimental period. No significant changes in body weight were observed across the groups (Control, A1, and AMD3100), indicating neither treatment-induced toxicity nor systemic effects on overall mouse health. Data are shown as mean ± SD, with "ns" denoting no significant difference. (D) Survival rate analysis for the three groups over 60 days after tumor inoculation. Mice in the Control group had the shortest survival, while those in the A1 group showed significantly extended survival, followed by AMD3100. Statistical comparisons between groups are shown with corresponding *p*-values (Control vs. AMD3100, *p* = 0.0011; Control vs. A1, *p* = 0.0005; AMD3100 vs. A1, *p* = 0.0434)

also negative. In the group treated with A1, there were inflammatory lesions with infiltration of mononuclear inflammatory cells around the portal space and the vessels, and it is noteworthy that the intensity of inflammation was lower in this group. Also, there was no evidence of fibrosis in the liver, and hepatocytic degeneration was negative.

Cytotoxicity outcomes demonstrate that while administration of the A1 compound at 5 mg/kg did not significantly alter serum ALT and AST levels compared to the control group, treatment with AMD3100 resulted in a notable increase in serum ALT and AST levels, indicating potential

hepatotoxicity. The histopathological examination further supported these findings, showing inflammatory lesions in both treatment groups, albeit with varying intensities, while no evidence of fibrosis or hepatocytic degeneration was observed. These findings indicate the importance of further investigation into the potential hepatotoxic effects of AMD3100 for clinical consideration.

## Discussion

Evidence demonstrated that the CXCL12/CXCR4 axis could be involved in the pathogenesis of several disorders [9, 10, 36, 37]. This axis also plays a crucial role in CRC

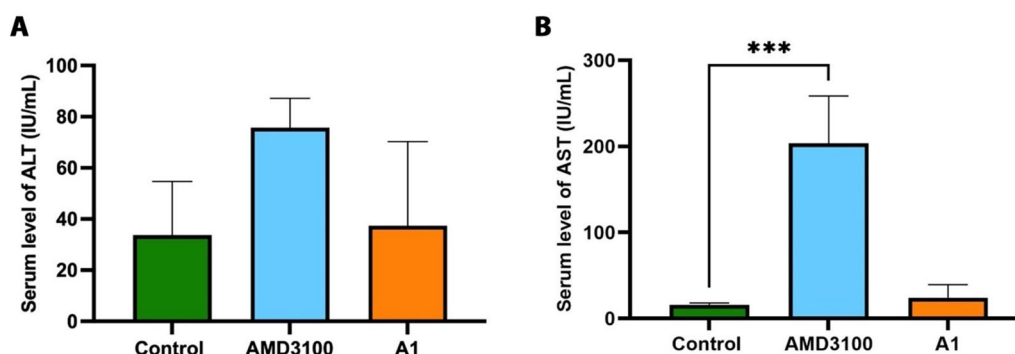


**Fig. 14** Comparative analysis of serum ALT (A) and AST (B) levels in different groups of BALB/C mice. The chart delineates the serum levels of alanine aminotransferase (ALT) and aspartate aminotransferase (AST) in various experimental cohorts of BALB/C mice, thereby providing insights into hepatic function and potential hepatotoxicity. The experiments were performed in duplicate, and the data are presented as Mean  $\pm$  Standard Deviation (SD). Statistical significance is denoted by \*\*\* $P < 0.0001$ , underscoring the significant differences in ALT and AST levels among the groups. These findings furnish a comparative assessment of liver enzyme levels, which serve as critical indicators of hepatic health and damage, potentially elucidating the systemic effects of the treatments under investigation. Error bars illustrate the standard deviation, accentuating consistency across replicates

immunopathology through the proliferation and migration of tumor cells and the angiogenesis and metastasis of CRC cells to the liver and lungs [5, 38]. Therefore, inhibiting the CXCR4 receptor can be one of the critical strategies in controlling the progression of CRC. Several studies have been conducted to inhibit the CXCR4 receptor in CRC. For example, the drug AMD3100 is known as a CXCR4 antagonist, and previous studies have shown that it can reduce the migration of cancer cells [39]. However, there are still challenges in CXCR4 receptor inhibition in CRC. Among the problems that have arisen are resistance to treatment and side effects of drugs. Moreover, more studies are needed to prove the efficacy and side effects of CXCR4 inhibitor drugs in humans [40].

Root means square deviation (RMSD) plots of the studied complexes show that the complexes were stable during simulations. However, it takes longer for the receptor in the complex with ITD to reach a steady state (Supplementary Information, Figure S4). Also, the RMSD plots of the ligands reveal higher stability of A1 and ITD in the receptor binding groove than that of AMD3100. While the protein conformation is considered rigid during the docking studies procedure, MDs enable more realistic structural studies of the complex's studies through its dynamic nature. According to the RMSF plot analysis, CXCR4 key interaction participant residues show minor fluctuations when interacting with A1 in the binding pocket. This is attributed to establishing more stable interactions that limit their fluctuations (Supplementary Information, Figure S5). CXCR4 binding groove residues form further molecular interactions with A1, which increase the binding affinity compared to those observed in the docking studies. Presence of dimethylphenyl

methanimine segments in A1 chemical structure enables formation of an electrostatic interaction network in the groove via  $\pi$ -Alkyl (A34, A89, W102, V112, and H113),  $\pi$ -Cation (Y116) as well as  $\pi$ - $\pi$  T-Shaped interactions that sandwiches the second segment between residues W94 and H113 with the contribution of the first dimethylphenyl methanimine as well (Fig. 15 and Supplementary Information, Figure S8 and Table S1). While A1 interacts with the groove entrance residues mainly through electrostatic interactions, the compound interacts with the depth of the groove participant residues through hydrogen and halogen bond formation and attractive charge interactions (Y116, S285, E288).

Similar electrostatic interactions are also observed when ITD interacts with the binding pocket, which was not observed when employing molecular docking studies.  $\pi$ -Alkyl (A94, W102, and H113),  $\pi$ -Sulfur (Y113) and  $\pi$ - $\pi$  stacked interactions with W94 help localization of ITD in the groove. While those salt-bridge interactions with residue D97 observed through docking studies are lost, attractive charge interactions and hydrogen bonds with residues E288 and R188 were stable during MDs. The absence of electrostatic interactions in the AMD3100-CXCR4 complex results in the significantly lower affinity of the ligand for the receptor in comparison with those of A1 and ITD ( $-31.53 \pm 5.66$  kcal/mol). The compound forms attractive charge interactions, and hydrogen bonds with residues E288 and R188 were stable during MDs to stay in the binding groove.

The binding free energies of the studied compounds for CXCR4 were measured using the MMPBSA script. In contrast, the contribution of electrostatic energy, van der Waals energy, and apolar and polar solvation energy

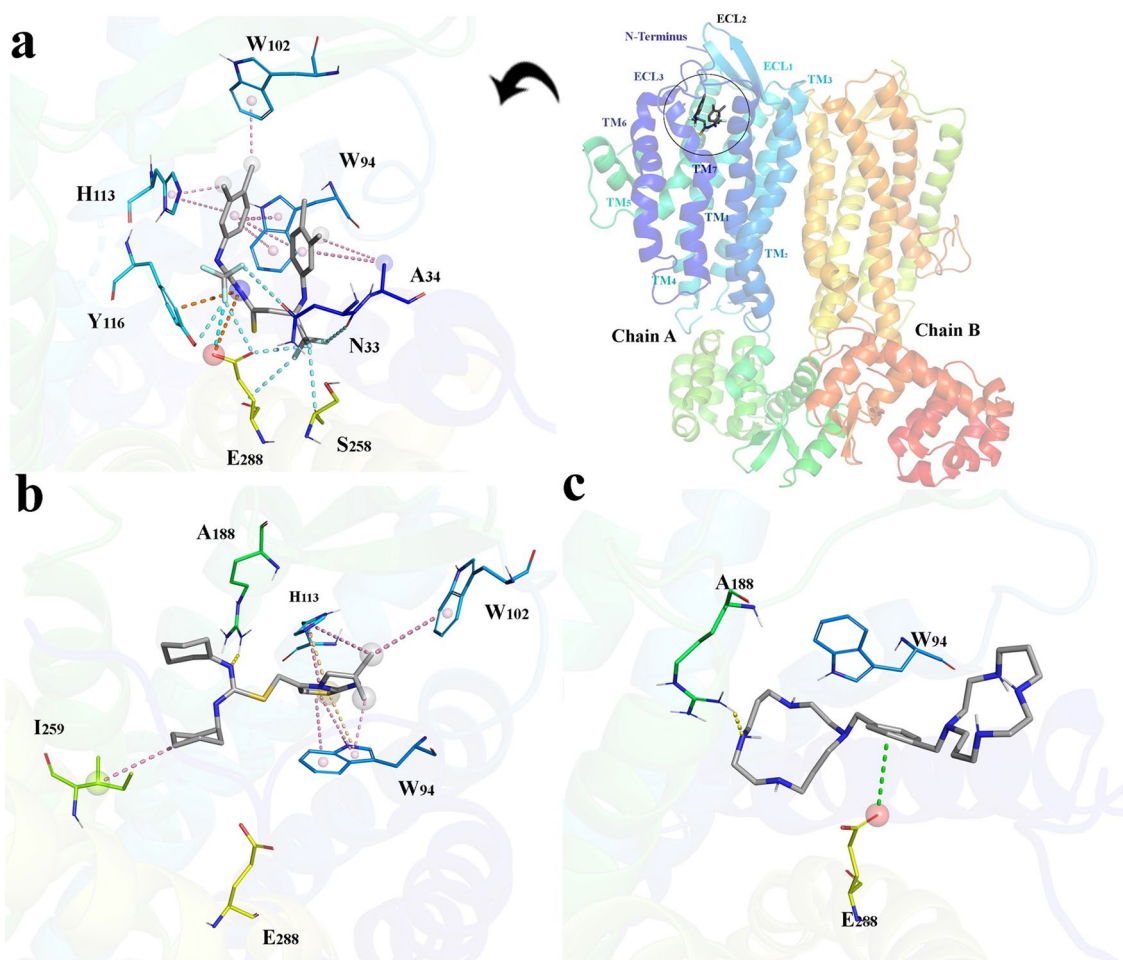


**Fig. 15** The overall structure of CXCR4 (dimer) and the CXCR4 binding site (groove) for CXCL12, and the inhibitors binding pocket as well as a close view of the studied ligands interactions in the CXCR4 binding pocket; **a.** A1, **b.** ITD and **c.** AMD3100. Green dashes represent salt bridges, velvet dashes represent  $\pi$ - $\pi$  electrostatic interactions, orange dashes represent  $\pi$ -cation and  $\pi$ -anion interactions, yellow dashes represent conventional hydrogen bonds, and light blue dashes represent halogen bonds

were considered. The binding free energies were calculated assuming a timeframe of 20 ns (1–20, 20–40, 40–60, 60–80, and 80–100 ns) throughout the simulation time (Supplementary Information, Figure S6 and Table S2). Accordingly, a descending trend was observed in the  $\Delta G$  value calculated for A1, while those of ITD and AMD3100 deviate. Per-residue energy decomposition analysis shows that W94, Y113, Y116, D184, and F292 have the highest energy contributions in the target binding energy for CXCR4 (Supplementary Information, Figure S7). To summarize, it is inferred that electrostatic interactions play a critical role in the interactions of the studied ligand with the CXCL12/CXCR4 binding site.

The expression level of the *CXCR4* gene in CT-26 cells was significantly higher than in normal MEF cells, which is in line with a study by Is [28] where the RT-PCR method showed the *CXCR4* receptor expression in

CT-26 cells [41]. Besides the results obtained through *in silico* and *in vitro* studies, A1 showed good cytotoxic properties against CT-26 cell lines at 12.5 to 400  $\mu\text{g/ml}$  concentrations. AMD3100 did not significantly affect cell viability from 12.5 to 800  $\mu\text{g/ml}$  concentrations in CT-26 cell lines [17]. A significant decrease in cell proliferation was observed at a concentration of 40  $\mu\text{g/ml}$  A1 after 72 h of treatment, indicating that A1 significantly inhibits CT-26 cell growth. Compared to AMD3100, A1 had a better anti-proliferative effect on CT-26 cells, which was also statistically significant. Previous studies showed a substantial impact of CXCL12 on the proliferation of CXCR4<sup>+</sup> Ewing’s sarcoma cells under serum deprivation conditions. The study above disrupted this proliferative effect when cells were treated with AMD3100 *in vitro* [42, 43]. Another study performed on SW480 cells showed that cell viability was significantly suppressed in

a dose-dependent manner by AMD3100. AMD3100 at 100 and 1000 ng/mL significantly inhibited the invasive ability of SW480 cells [44]. In contrast, another study in BHP10-3 and BHP10-3 M cells showed that blocking CXCR4 with AMD3100 from 1 to 100 ng/ml did not suppress cell proliferation in either cell line [45].

Functional assays were used to confirm the binding of the drug to the CXCR4 receptor. The results showed that treating CT-26 cells with 100 ng/ml CXCL12 for 72 h significantly increased the expression of the CXCR4 receptor gene compared to the untreated control group. Also, treatment of CT-26 cells with 60 µg/ml A1 and 100 ng/ml CXCL12 decreased CXCR4 gene expression compared to the group treated with only 100 ng/ml CXCL12, although this decrease was not statistically significant. These results show that A1 has cytotoxic activity in doses higher than the  $IC_{50}$  dose and affects cell proliferation and CXCR4 receptor expression in amounts lower than the  $IC_{50}$  dose. As a result, A1 has a dual cytotoxic and antiproliferative function, which increases its potential and rationale for its use in cancer treatment. Other CXCR4 inhibitor drugs with double action have been introduced in this field. In this regard, a new CXCR4 inhibitor modified with picolinamide scaffold (CPZ1344) was designed and synthesized, and its anticancer function was evaluated in glioblastoma. This study showed that CPZ1344 decreased the growth of glioblastoma cells dose-dependently [46].

Moreover, analysis of flow cytometry results showed that CXCR4<sup>+</sup> CT-26 cells were reduced when exposed to a combination of 60 µg/ml A1 and 100 ng/ml CXCL12 for 72 h. These findings highlight the potential of A1 as a therapeutic option to regulate CXCR4-related processes in the CT-26 cell line [47]. However, further research is necessary to fully understand the underlying mechanism of this interaction and its implications for therapeutic applications. Studies showed that following the binding of CXCL12 to CXCR4 and the activation of the Gai-related pathway, the cellular levels of cAMP decrease, and in this way, the function of the drug and its binding to the CXCR4 receptor can be confirmed indirectly [48]. Findings showed that the group treated with concentrations of 100 and 1000 nmol/ml A1 along with 100 ng/ml CXCL12 and 5 µM/ml forskolin significantly increased cAMP levels compared to the control group. Correspondingly, the drug AMD3100 at a concentration of 1000 nmol/ml increased the level of cAMP, which was statistically significant compared to the control group. These results also showed that A1 in concentrations similar to AMD3100 with better performance can increase intracellular cAMP production. A study in this field reported that inhibition of CXCR4 with the inhibitor MSX-122 compared to AMD3100 had better

performance in inhibiting CXCR4 and increasing cAMP levels, consistent with the present study [29]. In addition, this study showed that A1 and AMD3100 can inhibit the CXCL12/CXCR4 downstream signals by CXCR4, which inhibits the phosphorylation of pAKT, one of the most critical adaptor molecules in the pathway. In this regard, other studies reported that blocking CXCR4 by CXCR4 inhibitors, such as AMD3100 and BPRCX807, could reduce the expression of pAKT [49, 50].

T140 analogs as CXCR4 antagonists inhibit CXCL12-induced migration of breast cancer, leukemia, and endothelial cells in vitro in a manner associated with tumor spread and angiogenesis [51]. Another study demonstrated the ability of AMD3100 to reduce AKT ERK1 and ERK2 activation, all of which are pathways downstream of CXCR4 that increase cell survival, proliferation, and migration [52]. Our results showed that the percentage of migrating CT-26 cells after treating the cells with 10 µM/ml of both A1 and AMD3100 compounds was significantly reduced compared to the control group. However, this reduction was more remarkable for the AMD3100. These results show that in line with the studies mentioned in this field, both A1 and AMD3100 compounds can disrupt and reduce the mechanisms related to cell migration by inhibiting the CXCR4 receptor in competition with CXCL12.

In CRC, the density of infiltrating lymphocytes at the tumor margin can predict the response to chemotherapy, and a high percentage of CD4<sup>+</sup> or CD8<sup>+</sup> Tregs is associated with shorter survival [53, 54]. As a result, inhibiting the recruitment and infiltration of these cells through blocking the CXCR4/CXCL12 axis can be therapeutically effective. This study showed that the percentage of Tregs in the tumor tissue and the spleen of mice treated with AMD3100 and A1 decreased significantly compared to the control group. These results show that the drug AMD3100 works better than the A1 with a slight difference, as observed in the cell migration test in vitro. One of the most significant effects of inhibition of the CXCL12/CXCR4 axis inhibition has been the selective reduction of the infiltration of Tregs within the tumor by converting them into helper-like T cells [55]. Another study showed that AMD3100 could reduce PD-1 expression in intratumoral CD8<sup>+</sup> T cells and recycle Tregs into helper-like T cells [56].

In the present study, the effect of A1 and AMD3100 compounds on the expression of genes involved in angiogenesis and tumor growth, including *CXCR4*, *VEGF*, and *FGF*, as well as cytokine genes related to Tregs, including *IL-10* and *TGF-β*, in the tumor tissue of mice. The results showed that the expression of the *CXCR4* gene was decreased in both groups treated with A1 and AMD3100 compared to the control group,

although it was not statistically significant. A study has shown that CXCR4 receptor inhibition using AMD3100 can reduce the expression of *cathepsin K*, *Runx2*, *CXCL12*, and *RANKL* at the mRNA level [57]. Based on this and considering the role of CXCL12 in increasing the expression of CXCR4, which takes place through the MEK/ERK signaling pathway as well as the NF $\kappa$ B factor, it may be able to reduce CXCR4 expression indirectly [47].

Furthermore, *FGF* gene expression increased in the groups treated with A1 and AMD3100 compared to the control group; however, this difference was not statistically significant. In this case, a study has shown that FGF through miR31 can reduce the expression of *CXCL12* at the mRNA level [58]. As a result, the reduction of FGF is not always in favor of the treatment, and this increase in expression may lead to inhibiting the growth, proliferation, and migration of tumor cells by inhibiting the expression of CXCL12, as well as reducing the infiltration of inhibitory cells in the TME. In the case of *VEGF*, the results were the opposite, so in the groups treated with A1 and AMD3100, there was a decrease in expression at mRNA and protein levels compared to the control group. Nevertheless, this difference between the groups was significant only for those treated with the A1. These results show that A1 and AMD3100 may interfere with angiogenesis by inhibiting VEGF expression.

A study in this field reported that in a xenograft mouse model of chondrosarcoma, four weeks of treatment with AMD3100 (1.25 mg/kg, intraperitoneally twice daily) inhibited tumor angiogenesis, tumor growth, and metastasis. Additionally, the expression of VEGFA in tumor tissue was significantly reduced following the treatment [59]. Investigating the role of CXCL12/CXCR4 signaling in resistance to anti-VEGFR2 treatment in SL4 and CT-26 models showed that AMD3100 therapy significantly enhanced the antitumor effect of DC101 treatment as VEGF receptor 2 (VEGFR2) inhibitor, which delayed tumor growth and increased animal survival [60].

Regarding the expression of *IL-10* and *TGF- $\beta$*  genes, the results showed that the expression of these genes as cytokine products of Tregs in the groups treated with A1 and AMD3100 significantly decreased compared to the control group. These results were also valid for IL-10 and TGF- $\beta$  protein levels. Despite the more significant decrease in the levels of these cytokines in the group treated with A1 compared to the AMD3100 and control groups, the difference was not significant. These findings show that A1, in addition to inhibiting the infiltration of Tregs, can also disrupt their function in tumor tissue. In line with these results, other studies have also shown that by inhibiting CXCR4, the tissue or systemic levels of IL-10 and TGF- $\beta$  are reduced

at the mRNA and protein level, which can lead to the improvement and stimulation of antitumor responses of the immune system [61, 62].

The effect of A1 and AMD3100 on tumor size and the survival of treated animals compared to the control group were measured. The results showed that the difference in tumor size in the control, AMD3100, and A1 groups became significant over time. The average tumor size in the control group on the last day of treatment (day 33) was greater than that of the AMD3100 and A1 groups on the same day, which indicates that the A1 was more successful in reducing the tumor size than the group treated with AMD3100 [63]. The survival results showed a significant percentage difference between the three groups. Furthermore, the median survival value for the control group was 36.5, the AMD3100 group was 47.5, and the A1 group was 53.5 days. Studies in this field have also reported that inhibiting CXCR4 with AMD3100 can lead to increased survival of CRC model mice [64].

Collectively, the mechanistic rationale for the observed regulation of CXCR4 upon A1 and AMD3100 treatment in CRC involves inhibiting tumor cell proliferation [65, 66] and migration [67], modulation of the immune response within the TME [67, 68], and other potential anti-tumor therapeutic efficacy of A1 [17, 60, 69].

In terms of toxicity and side effects, the results of the serum levels of ALT and AST liver enzymes showed that treating mice with the drug AMD3100 can lead to an increase in the damage of liver cells and the enzymes released from them. In this respect, A1 performed better, and in the histopathological examination, A1 caused less inflammation in the liver tissue. Therefore, A1 is safer than AMD3100, at least in terms of hepatotoxicity. Some studies have reported that the toxicities caused by AMD3100 were limited, and all were only grade 1 based on the WHO scale. The most common general toxicity was erythema or edema at the injection site, experienced by ten patients, which did not require treatment. The most common noncutaneous toxicities considered possibly or probably related to the study drug were gastrointestinal. A study showed that treatment of mice with AMD3100 in a chronic CCl<sub>4</sub>-induced liver injury model led to increased liver inflammation and fibrosis with a particular increase in intrahepatic neutrophils. Furthermore, in an acute CCl<sub>4</sub>-induced liver injury model, AMD3100 resulted in increased intrahepatic neutrophil counts and a tendency toward worsening necrosis [70]. Findings regarding the side effects of AMD3100 are contradictory, but in the present study, liver damage was evident following the use of this drug in BALB/c mice.

### Limitations and future directions

Despite the encouraging outcomes, several obstacles need recognition, highlighting essential avenues for future study. The research primarily used the murine CT-26 CRC cell line, which could fail to represent the complexity and variability of human colorectal malignancies adequately. Future research should corroborate these findings with human cell lines, namely HCT116 and SW480, to improve the applicability of the results. Moreover, although a well-established model, using BALB/c mice presents difficulties in precisely mirroring the immune and tumor microenvironment responses seen in humans. Integrating more therapeutically relevant models, such as humanized mice or patient-derived xenografts, would enhance the application of the results in human situations. The limited sample size in the animal trials may have restricted statistical power; hence, larger cohorts are recommended for future investigations to get more certain findings. This research broadly examined short-term results, including tumor size reduction and survival, while neglecting long-term impacts, such as tumor recurrence and metastasis. Future studies must examine these long-term impacts to assess A1's viability as a sustainable therapeutic alternative. The work offers substantial insights into A1's therapeutic benefits; nonetheless, more mechanistic investigations are essential. Subsequent investigations should examine more molecular pathways and downstream consequences of CXCR4 inhibition to clarify the function of A1 in tumor suppression comprehensively. Exploring combination medicines that integrate A1 with known treatments like chemotherapy or immune checkpoint inhibitors may have synergistic effects, increasing effectiveness and boosting patient outcomes. Finally, early-phase clinical studies are crucial for evaluating the pharmacokinetics, safety, and therapeutic efficacy of A1 in human participants. Extensive preclinical validation, including patient-derived xenograft models, will be essential in assessing the effectiveness of A1 in more therapeutically relevant contexts.

### Conclusion

A computational evaluation of A1, AMD3100, and ITD interactions over the CXCR4 receptor further confirmed the tighter and more stable intercalations of A1 in complex with the receptor. Also, A1 has significantly reduced the proliferation of CT-26 cells treated with CXCL12. Furthermore, co-treatment of A1 and CXCL12 dramatically reduced the number of CXCR4<sup>+</sup> cells. These observations suggest that A1 has potential therapeutic implications in regulating the proliferation and expression of the CXCR4 receptor in CT-26 cells. A1 inhibits cell migration, essential in treating metastatic cancers such as CRC. By inhibiting

CXCR4, the compound decreases the infiltration of micro-environmental Tregs in the TME, eventually disrupting the function of these cells and reducing the expression of IL-10 and TGF- $\beta$  cytokines. A1 efficiently reduced tumor size and increased survival rate in vivo and shows acceptable hepatotoxicity compared to AMD3100. Despite the satisfactory results in comparing A1 and AMD3100 as well-known and tested compounds in clinical studies, more investigations of different cancer cell lines and clinical phases are required.

### Supplementary Information

The online version contains supplementary material available at <https://doi.org/10.1186/s12935-024-03584-y>.

Supplementary material 1 .

### Acknowledgements

This study was supported by Iran University of Medical Sciences and Rafsanjan University of Medical Sciences.

### Author contributions

HKH; Study design, draft preparation, experiments, Revisions, KB; Molecular docking studies and analysis; AR; Experiments, AN; Experiments, ES; Study design, supervision, GHH; draft editing, MKH; Data analysis, MK; Experiments, AD; The compound synthesis and analysis, RF; Study design, supervision, final editing.

### Funding

This study was funded by Iran University of Medical Sciences and Rafsanjan University of Medical Sciences, with Grant Numbers (1400-3-4-22138) and (401104).

### Availability of Data and Materials

No datasets were generated or analysed during the current study.

### Declarations

#### Ethics approval and Consent to Participate

BALB/C mice were used in this study following ethical guidelines, and no human samples were involved. The Iran University of Medical Sciences Ethics Committee approved the experimental procedures under the approval code IR.IUMS.FMD.REC.1400.590.

#### Competing interests

The authors declare no competing interests.

#### Author details

<sup>1</sup>Department of Immunology, School of Medicine, Rafsanjan University of Medical Sciences, Rafsanjan, Iran. <sup>2</sup>Department of Immunology, School of Medicine, Iran University of Medical Sciences, Hemmat Ave, Tehran, Iran. <sup>3</sup>Eye Research Center, the Five Senses Health Institute, Rassoul Akram Hospital, University of Medical Sciences, Tehran, Iran. <sup>4</sup>Immunology Research Center, Iran University of Medical Sciences, Tehran, Iran. <sup>5</sup>Department of Chemistry, Faculty of Science, Vali-E-Asr University of Rafsanjan, Rafsanjan, Iran. <sup>6</sup>Molecular Medicine Research Centre, Institute of Basics Medical Sciences, Rafsanjan University of Medical Sciences, Rafsanjan, Iran.

Received: 8 July 2024 Accepted: 22 November 2024

Published online: 05 January 2025

## References

- Hossain MS, et al. Colorectal cancer: a review of carcinogenesis, global epidemiology, current challenges, risk factors, preventive and treatment strategies. *Cancers*. 2022;14(7):1732.
- Chandel D, et al. Isolation, characterization and identification of antigenotoxic and anticancerous indigenous probiotics and their prophylactic potential in experimental colon carcinogenesis. *Sci Rep*. 2019;9(1):14769.
- Martin FL, et al. Age-related and gender-related increases in colorectal cancer mortality rates in Brazil between 1979 and 2015: projections for continuing rises in disease. *J Gastrointest Cancer*. 2021;52:280–8.
- Siegel RL, et al. Colorectal cancer statistics, 2023. *CA Cancer J Clin*. 2023;73(3):233–54.
- Khare T, Bissonnette M, Khare S. CXCL12-CXCR4/CXCR7 axis in colorectal cancer: Therapeutic target in preclinical and clinical studies. *Int J Mol Sci*. 2021;22(14):7371.
- Goïta AA, Guenot D. Colorectal cancer: the contribution of CXCL12 and its receptors CXCR4 and CXCR7. *Cancers*. 2022;14(7):1810.
- Khorramdelazad H, et al. New insights into the role of stromal cell-derived factor 1 (SDF-1/CXCL12) in the pathophysiology of multiple sclerosis. *J Neuroimmunol*. 2016;290:70–5.
- Aminzadeh F, et al. Differential expression of CXC Chemokines CXCL 10 and CXCL 12 in Term and Pre-term Neonates and Their Mothers. *Am J Reprod Immunol*. 2012;68(4):338–44.
- Bagheri V, et al. CXCL12 and CXCR4 in the peripheral blood of patients with Parkinson's disease. *NeuroImmunomodulation*. 2019;25(4):201–5.
- Azin H, et al. The SDF-1 3' a genetic variation of the chemokine SDF-1 $\alpha$  (CXCL12) in parallel with its increased circulating levels is associated with susceptibility to MS: a study on Iranian multiple sclerosis patients. *J Mol Neurosci*. 2012;47:431–6.
- Hassanshahi G, et al. Assessment of CXCL12 (SDF-1 $\alpha$ ) polymorphisms and its serum level in posttransfusion occult HBV-infected patients in Southeastern Iran. *Arch Med Res*. 2010;41(5):338–42.
- Nazari A, Khorramdelazad H, Hassanshahi G. Biological/pathological functions of the CXCL12/CXCR4/CXCR7 axes in the pathogenesis of bladder cancer. *Int J Clin Oncol*. 2017;22:991–1000.
- Bocchi M, et al. Involvement of CXCL12/CXCR4 axis in colorectal cancer: a mini-review. *Mol Biol Reports*. 2023. <https://doi.org/10.1007/s11033-023-08479-1>.
- Yang Y, et al. CXCL12-CXCR4/CXCR7 axis in cancer: from mechanisms to clinical applications. *Int J Biol Sci*. 2023;19(11):3341.
- Biasci D, et al. CXCR4 inhibition in human pancreatic and colorectal cancers induces an integrated immune response. *Proc Natl Acad Sci*. 2020;117(46):28960–70.
- Smoragiewicz M. Modulation of the tumor microenvironment by the CXCR4 antagonist AMD3100 in pancreatic and colorectal adenocarcinoma. Cambridge: University of Cambridge; 2019.
- Khorramdelazad H, et al. Antitumor activities of a novel fluorinated small molecule (A1) in CT26 colorectal cancer cells molecular docking and in vitro studies. *J Biomol Struct Dyn*. 2023. <https://doi.org/10.1080/07391102.2023.2256406>.
- Berendsen HJ, van der Spoel D, van Drunen R. GROMACS: A message-passing parallel molecular dynamics implementation. *Comput Phys Commun*. 1995;91(1–3):43–56.
- Pérez A, et al. Refinement of the AMBER force field for nucleic acids: improving the description of  $\alpha/\gamma$  conformers. *Biophys J*. 2007;92(11):3817–29.
- Bussi G, Donadio D, Parrinello M. Canonical sampling through velocity rescaling. *J Chem Phys*. 2007. <https://doi.org/10.1063/1.2408420>.
- Parrinello M, Rahman A. Polymorphic transitions in single crystals: A new molecular dynamics method. *J Appl Phys*. 1981;52(12):7182–90.
- Darden T, York D, Pedersen L. Particle mesh Ewald: An N<sup>3</sup> log(N) method for Ewald sums in large systems. *J Chem Phys*. 1993;98(12):10089–92.
- Hess B, et al. LINCS: A linear constraint solver for molecular simulations. *J Comput Chem*. 1997;18(12):1463–72.
- Kumari R, et al. g\_mmpbsa A GROMACS tool for high-throughput MM-PBSA calculations. *J Chem Inf Model*. 2014;54(7):1951–62.
- Biovia DS, Dsme R. San Diego: Dassault Systèmes. Release. 2015;1.4.
- Humphrey W, Dalke A, Schulten K. VMD: visual molecular dynamics. *J Mol Graph*. 1996;14(1):33–8.
- W.L., D.L. An informal Newsletter associated with the BBSRC Collaborative Computational Project No. 4 on Protein Crystallography CCP4 newsletter, On Protein Crystallography. . 2002; <https://legacy.ccp4.ac.uk/newsletters/newsletter41.pdf>.
- Kazemi E, Darehkordi A, Abbasi A. Friedel-Crafts synthesis of bis (trifluoromethylated)-4-aryl-3, 4-dihydroquinazolines, bis (trifluoromethylated)-3, 4-dihydroquinazoline-4-ols and trifluoromethyl arylketoinimes using N-aryltrifluoroacetimidoyl chlorides and benzene derivatives. *Mol Divers*. 2021. <https://doi.org/10.1007/s11030-021-10189-4>.
- Liang Z, et al. Development of a unique small molecule modulator of CXCR4. *PLoS ONE*. 2012;7(4): e34038.
- Smith-Berdan S, et al. Acute and endothelial-specific Robo4 deletion affect hematopoietic stem cell trafficking independent of VCAM1. *PLoS ONE*. 2021;16(8): e0255606.
- Wu S, et al. miR-126 downregulates CXCL12 expression in intestinal epithelial cells to suppress the recruitment and function of macrophages and tumorigenesis in a murine model of colitis-associated colorectal cancer. *Mol Oncol*. 2022;16(19):3465–89.
- Yu X, et al. CXCL12/CXCR4 promotes inflammation-driven colorectal cancer progression through activation of RhoA signaling by sponging miR-133a-3p. *J Exp Clin Cancer Res*. 2019;38:1–18.
- Kouvaras E, et al. Hypoxia-inducible factor 1- $\alpha$  and vascular endothelial growth factor in cartilage tumors. *Biotech Histochem*. 2019;94(4):283–9.
- Institutional Animal Care and Use Committee. <https://iacuc.wsu.edu/guidelines/>. Accessed 12 Dec 2023
- Rodallec A, et al. Tumor growth monitoring in breast cancer xenografts: A good technique for a strong ethic. *PLoS ONE*. 2022;17(9): e0274886.
- Bagheri V, et al. CXC chemokine CXCL12 tissue expression and circulating levels in peptic ulcer patients with *Helicobacter pylori* infection. *Cytokine*. 2016;85:1–4.
- Ferdousie VT, et al. Serum CXCL10 and CXCL12 chemokine levels are associated with the severity of coronary artery disease and coronary artery occlusion. *Int J Cardiol*. 2017;233:23–8.
- Wang D, et al. Exosome-encapsulated miRNAs contribute to CXCL12/CXCR4-induced liver metastasis of colorectal cancer by enhancing M2 polarization of macrophages. *Cancer Lett*. 2020;474:36–52.
- Zhu WB, Zhao ZF, Zhou X. AMD3100 inhibits epithelial–mesenchymal transition, cell invasion, and metastasis in the liver and the lung through blocking the SDF-1 $\alpha$ /CXCR4 signaling pathway in prostate cancer. *J Cell Physiol*. 2019;234(7):11746–59.
- Balkwill FR. The chemokine system and cancer. *J Pathol*. 2012;226(2):148–57.
- Is Z. The chemokine receptor CXCR4 is required for outgrowth of colon carcinoma micrometastasis. *Cancer Res*. 2003;62:3833–9.
- Berghuis D, et al. The CXCR4-CXCL12 axis in Ewing sarcoma: promotion of tumor growth rather than metastatic disease. *Clin Sarcoma Res*. 2012;2:1–9.
- Liao Y-X, et al. AMD3100 reduces CXCR4-mediated survival and metastasis of osteosarcoma by inhibiting JNK and Akt, but not p38 or Erk1/2, pathways in in vitro and mouse experiments. *Oncol Rep*. 2015;34(1):33–42.
- Li J-K, et al. Inhibition of CXCR4 activity with AMD3100 decreases invasion of human colorectal cancer cells in vitro. *World J Gastroenterol*. 2008;14(15):2308.
- Jung YH, et al. Antitumor effect of CXCR4 antagonist AMD3100 on the tumorigenic cell line of BHP10-3 papillary thyroid cancer cells. *Head Neck*. 2016;38(10):1479–86.
- Luo Z, et al. Novel CXCR4 Inhibitor CPZ1344 Inhibits the Proliferation, Migration and Angiogenesis of Glioblastoma. *Pathol Oncol Res*. 2020;26:2597–604.
- Kukreja P, et al. Up-regulation of CXCR4 expression in PC-3 cells by stromal-derived factor-1 $\alpha$  (CXCL12) increases endothelial adhesion and transendothelial migration: role of MEK/ERK signaling pathway–dependent NF- $\kappa$ B activation. *Can Res*. 2005;65(21):9891–8.
- Dwinell MB, et al. SDF-1/CXCL12 regulates cAMP production and ion transport in intestinal epithelial cells via CXCR4. *Am J Physiol-Gastrointest Liver Physiol*. 2004. <https://doi.org/10.1152/ajpgi.00112.2003>.
- Zhou J, et al. CXCR4 antagonist AMD3100 reverses the resistance to tamoxifen in breast cancer via inhibiting AKT phosphorylation. *Mol Ther-Oncolytics*. 2020;18:161–70.

50. Song J-S, et al. A highly selective and potent CXCR4 antagonist for hepatocellular carcinoma treatment. *Proc Natl Acad Sci.* 2021;118(13): e2015433118.
51. Burger M, et al. Small peptide inhibitors of the CXCR4 chemokine receptor (CD184) antagonize the activation, migration, and antiapoptotic responses of CXCL12 in chronic lymphocytic leukemia B cells. *Blood.* 2005;106(5):1824–30.
52. Redjal N, et al. CXCR4 inhibition synergizes with cytotoxic chemotherapy in gliomas. *Clin Cancer Res.* 2006;12(22):6765–71.
53. Halama N, et al. Localization and density of immune cells in the invasive margin of human colorectal cancer liver metastases are prognostic for response to chemotherapy. *Can Res.* 2011;71(17):5670–7.
54. Katz SC, et al. Regulatory T cell infiltration predicts outcome following resection of colorectal cancer liver metastases. *Ann Surg Oncol.* 2013;20:946–55.
55. Li B, et al. AMD3100 augments the efficacy of mesothelin-targeted, immune-activating VIC-008 in mesothelioma by modulating intratumoral immunosuppression. *Cancer Immunol Res.* 2018;6(5):539–51.
56. Zeng Y, et al. Dual blockade of CXCL12-CXCR4 and PD-1–PD-L1 pathways prolongs survival of ovarian tumor-bearing mice by prevention of immunosuppression in the tumor microenvironment. *FASEB J.* 2019;33(5):6596.
57. Ongprakobkul N, et al. Effects of local vs systemic administration of CXCR4 inhibitor AMD3100 on orthodontic tooth movement in rats. *Am J Orthod Dentofac Orthop.* 2022;162(2):182–92.
58. Itkin T, et al. FGF-2 expands murine hematopoietic stem and progenitor cells via proliferation of stromal cells, c-Kit activation, and CXCL12 down-regulation. *Blood, J Am Soc Hematol.* 2012;120(9):1843–55.
59. Sun X, et al. CXCR4-targeted therapy inhibits VEGF expression and chondrosarcoma angiogenesis and metastasis. *Mol Cancer Ther.* 2013;12(7):1163–70.
60. Jung K, et al. Targeting CXCR4-dependent immunosuppressive Ly6Clow monocytes improves antiangiogenic therapy in colorectal cancer. *Proc Natl Acad Sci.* 2017;114(39):10455–60.
61. Meiron M, et al. CXCL12 (SDF-1 $\alpha$ ) suppresses ongoing experimental autoimmune encephalomyelitis by selecting antigen-specific regulatory T cells. *J Exp Med.* 2008;205(11):2643–55.
62. Karpisheh V, et al. The role of regulatory T cells in the pathogenesis and treatment of prostate cancer. *Life Sci.* 2021;284: 119132.
63. Domanska UM, et al. CXCR4 inhibition with AMD3100 sensitizes prostate cancer to docetaxel chemotherapy. *Neoplasia.* 2012;14(8):709–18.
64. Rabinovich-Nikitin I, et al. Chronic administration of AMD3100 increases survival and alleviates pathology in SOD1 G93A mice model of ALS. *J Neuroinflammation.* 2016;13:1–11.
65. Yi T, et al. Quantitative phosphoproteomic analysis reveals system-wide signaling pathways downstream of SDF-1/CXCR4 in breast cancer stem cells. *Proc Natl Acad Sci.* 2014;111(21):E2182–90.
66. Chetram MA, Odero-Marah V, Hinton CV. Loss of PTEN permits CXCR4-mediated tumorigenesis through ERK1/2 in prostate cancer cells. *Mol Cancer Res.* 2011;9(1):90–102.
67. Benedicto A, Romayor I, Arteta B. CXCR4 receptor blockage reduces the contribution of tumor and stromal cells to the metastatic growth in the liver. *Oncol Rep.* 2018;39(4):2022–30.
68. Liu Z, Wang J, Chen H. CXCR4 antagonist AMD3100 (Plerixafor) modulates immune responses in the tumor microenvironment. *Int J Cancer Clin Res.* 2021. <https://doi.org/10.2393/2378-3419/1410144>.
69. Alzahrani SO, et al. Trans-IV restriction a new configuration for metal bis-cyclam complexes as potent CXCR4 inhibitors. *Dalton Transact.* 2024. <https://doi.org/10.1039/D3DT01729J>.
70. Saiman Y, et al. Inhibition of the CXCL 12/CXCR 4 chemokine axis with AMD 3100, a CXCR 4 small molecule inhibitor, worsens murine hepatic injury. *Hepatol Res.* 2015;45(7):794–803.

## Publisher's Note

Springer Nature remains neutral with regard to jurisdictional claims in published maps and institutional affiliations.